MICROCONTROLLER-BASED DESIGN AND DEVELOPMENT OF A REAL-TIME BODY TEMPERATURE AND HEART RATE MONITORING SYSTEM

BENSON ONYAGI AYIEKO

MASTER OF SCIENCE

(Physics)

JOMO KENYATTA UNIVERSITY

OF

AGRICULTURE AND TECHNOLOGY

2024

Microcontroller-Based Design and Development of a Real-Time Body Temperature and Heart Rate Monitoring System

Benson Onyagi Ayieko

A Thesis Submitted in Partial Fulfillment of the Requirements for the Degree of Master of Science in Physics of the Jomo Kenyatta University of Agriculture and Technology

2024

DECLARATION

This thesis is my original work and has not been presented for a degree in any other University

Signature…….…….Date.....

Benson Onyagi Ayieko

This thesis has been submitted for examination with our approval as the University Supervisors

Signature…….…….Date.....

Dr. Calvine Fundi Ominde, PhD

JKUAT, Kenya

Signature…….…….Date.....

Dr. Anthony Joseph Kiroe, PhD

JKUAT, Kenya

DEDICATION

Dedicated to my loving family with great appreciation.

ACKNOWLEDGEMENT

Appreciation is expressed to my supervisors Dr. Ominde Calvine Fundi and Dr. Kiroe Anthony Joseph for helpful discussions, comments and guidance in the course of doing this research. My gratitude also goes to staff Department of Physics, Jomo Kenyatta University of Agriculture and Technology (JKUAT), Kenya with special mention of the post graduate coordinators and advisors Dr. J. Munyithya and Dr. S.W. Mugo for their immense help, numerous suggestions and critiquing of this work. I do not want to forget the four patients who put their lives at risk during the uncertain COVID-19 season for me to be able to collect data. Lastly, I honour and appreciate my dear family for giving me a humble time during my studies.

TABLE OF CONTENTS

LIST OF TABLES

LIST OF FIGURES

LIST OF SYMBOLS

$\boldsymbol{\theta_{HR}}$	Measured Heart Rate
$\boldsymbol{\theta_{T}}$	Measured Body Temperature

LIST OF APPENDICES

ACRONYMS AND ABBREVIATIONS

ADC	Analog to Digital Converter
ANN	Artificial Neural Network
API	Application Programming Interface
ASSP	Analog Sensor Signal Processor
B & A	Bland and Altman
BPM	Beats per Minute
BT	Body Temperature
CI	Confidence Interval
CoD	Coefficient of Determination
CV	Coefficient of Variance
ECG	Electrocardiogram/Electrocardiography
FOV	Field of View
HMS	Health Monitoring System
HR	Heart Rate
HRV	Heart Rate Variability
HTTP	Hypertext Transfer Protocol
IDE	Integrated Development Environment
IR	Infrared

IRT	Infrared Thermometer/Thermography
LAN	Local Area Network
LCD	Liquid Crystal Display
LoA	Limits of Agreement
PPG	Photoplethysmography
ROI	Region of Interest
SARS	Severe Acute Respiratory Syndrome
SD	Standard Deviation
TSP/IP	Transmission Control Protocal/ Internet Protocal
WHO	World Health Organization
RPM	Remote Patient Monitoring

ABSTRACT

Healthcare is an important need of the human population. Heart rate and body temperature are some of the critical parameters that are routinely measured whenever a patient arrives in hospital. The ability to monitor the two parameters ensures that proper healthcare is delivered early. Most health monitoring systems presently in use only work in offline mode and therefore critical that a system is developed to enable for the real time remote monitoring of the patient. In addition, numerous challenges still exist in healthcare services. These include prolonged time of examination of patients by the medical professionals, conventional patient data retrieval, and the cable media use of the medical equipment's used. We therefore propose a heart rate and body temperature monitoring system based on a microcontroller to alert health care professionals when these values are abnormal. This study aims at relieving the burden of medical professionals in monitoring the patient, improving the efficiency in taking patient data and minimizing the risk of misdiagnosis. The system will enable real time remote monitoring. To realize this, a prototype system is developed to analyze the behavior of the heart rate and body temperature of several patients. The prototype consists of the MLX90614 temperature sensor and the XD-58C photoplethysmography sensor that measure body temperature and heart rate of a patient, respectively; and controlled by the Arduino mega 2560 microcontroller board. The XD-58C sensor counts the heart rate for specific interval of time and estimates the beats per minute while the MLX90614 sensor measures the body temperature. Both data are sent to the Arduino microcontroller for analysis and transmission to the receiver. A wireless system is used to transmit the measured data to a remote location. Finally, the data is displayed on a Liquid Crystal Diode screen and computer at the receiving end for further processing and patient care. The study findings revealed a strong positive correlation between the prototype, the clinical thermometer and sphygmomanometer methods in measuring body temperature and heart rate respectively for all the four patients. The bias which represents the systematic error in the measurement was found to be within the medically predetermined a priori conditions of ±0.5°C and ±5 BPM for all cases under consideration. This confirmed that the prototype and gold standard methods used in measuring body temperature and heart rate were in agreement. As a result, the prototype can replace alternative methods of measurement in monitoring the two vital signs.

CHAPTER ONE

INTRODUCTION

1.1 Introduction

Health is a global challenge for humanity (Oleg et al., 2021). According to the World Health Organization (WHO) the highest attainable standard of health is a fundamental right for a human being (Karaduman, 2014). Presently, Health Monitoring Systems (HMS) can be used to continuously monitor our health status to ensure the human body is constantly maintained in good condition. Remote Patient Monitoring (RPM) is a technology that helps in the monitoring of a patient even when the patient is not within a medical facility. This increases access to health services and infrastructure while minimizing on cost. RPM saves time of both the patient and the physician, hence increasing efficiency and reliability of health services.

Body Temperature (BT), Heart Rate (HR), blood pressure, body weight, blood oxygen and glucose levels are some of the most fundamental vital signs for clinical diagnosis and daily healthcare (Youssef *et al*., 2020). These parameters can give some important indicator of the body's health condition. For instance, an unstable HR might indicate a cardiac problem while high temperatures may be an indication of a fever. This early sign is a good indicator for one to consult the doctor for further check-up. In this study, a microcontroller-based BT and HR remote monitoring system was developed.

Normal BT varies from person to person and changes throughout the day. BT is lowest in the early morning and highest in the early evening. The average normal BT is about 37℃. However, it can be as low as 36.1℃ in the early morning and as high as 37.8℃ and still be considered normal. Thus, the normal range for BT is 36.1℃ to 37.8℃. The physiological damages and fatality will occur when there is a difference of more than ±3.5°C from the normal BT (Balli *et al*., 2023; Geneva *et al*., 2019; Parsons, 2014).

BT can be measured in different locations on a human body using a thermometer. The most common places for measuring the BT are in the armpit, mouth, ear, and rectum (Parsons, 2014). According to (Geneva *et al*., 2019), the temperature value might be shown differently from different parts of human body, thus there is no single number that represents an exact value of normal temperature for different people under different conditions. There are a few intrinsic factors that affect human BT, such as ovulation, circadian rhythm, age, exercise and thyroid hormones. While for the skin temperature, the measurement is also affected by the ambient conditions.

Temperature can be measured by using different types of sensors. The sensors come in different forms such as Resistance Temperature Detectors (RTD), thermistors, thermocouples and Integrated Circuit (IC) sensors. In this study, BT was measured by use of an IR pyrometer that measures the skin temperature on the forehead of a patient.

Similar to BT, a normal resting HR also varies from person to person, depending on their age, gender, daily activity, fitness, body condition and medications that they take (Tiwari *et al*., 2021; Sammito and Böckelmann, 2016; Valentini and Parati, 2009). A normal resting HR for adult's ranges from 60 to 100 Beats per Minute (BPM) (Kansara *et al*, 2021; Avram *et al*., 2019; Valentini and Parati, 2009). HR is the number of times the heart contracts and relaxes in a unit of time (usually per minute). The functioning of the heart is considered as efficient if it is having lower HR when the patient is at rest. Babies have a much higher rate than adults about 120 BPM and older children have HR around 90 BPM (Gupta *et al*., 2009). If the HR is higher than the normal HR, it is an indication of a condition known as tachycardia and if the HR is lower than the normal HR, it is an indication of a condition known as bradycardia. In this study, HR was measured from the left finger by tightly placing the sensor on the tips of the finger and on the ring position.

This work describes the design of an autonomous patient monitoring prototype model based on Arduino technology to measure the BT and HR of a patient and sends the data to a remote end where it is displayed and the physician able to examine them. The device is of much help during emergency situations, for saving time of both the patient and doctor

and for containing the spread of opportunistic diseases including the novel COVID-19 virus, Mpox etc.

1.2 Problem Statement

There are several medical devices and HMS's available in the market today. These include Nike Fuel Band, Numera devices, IntelliVue MX40 and Bio Harness BT sensor devices. However, these systems are only able to work in offline mode. They also do not provide open-source software. In the offline mode the medical devices cannot autonomously monitor the vital signs under consideration for lack of an internet connection. There is therefore great need of developing HMS's that support real time monitoring. They should also be able to accommodate open-source software providing users with the rights to study, analyze or modify the software in case of need of improvement or change in technology. This work proposes a prototype BT and HR monitoring system to be developed. The prototype is based on the MLX90614 temperature and the XD-58C heart rate sensors. The MLX90614 is a noninvasive sensor that measures the intensity of the frequency of the energy emitted by the patient's body to determine its temperature. Similarly, the XD-58C is a PPG based sensor that measure the amount of IR light absorbed or reflected by blood to determine the HR. The processing and analysis of the sensor signals is done with the Arduino mega 2560, a microcontroller board (ATmega 2560) that executes its instructions in a single clock cycle. These attributes make the prototype suitable to investigate the behavior of the BT and HR of several patients in an effort to determine their health status. This will enhance the efficiency of medical personnel in monitoring patients. Shorten the time in taking patient data and minimize the risk of misdiagnosis.

1.2 Justification

HMS's face several challenges. These include, time involved to examine patients, conventional patient data retrieval system, among others. In this study we use the MLX90614 and XD-58C BT and HR sensors that have unique features that measure the

patient's BT and HR signals giving out unique parameters thus allowing for programming of HMS's and ease of improvement in cases of new technological advancement. The information obtained from this research is fundamental for mass production and optimization of HMS's for improved efficiency and mobility of patients.

1.3 Objectives

1.3.1 General Objective

To design and develop a real-time microcontroller-based human body temperature and heart rate monitoring system.

1.3.2 Specific Objectives

1. To develop a body temperature and heart rate prototype system using the MLX90614 and the XD-58C sensors for the measurement and evaluation of body temperature and heart rate status of patients.
2. To evaluate the relationship between the body temperature measurements made by the prototype and the clinical thermometer on patients.
3. To analyze the relation between heart rate measurements made by the sphygmomanometer and the prototype on patients.
4. To design a feedforward-feedback multilayer body temperature and heart rate model based on a microcontroller system for the measurement and analysis of body temperature and heart rate of patients.

CHAPTER TWO

LITERATURE REVIEW

2.1 Related Work

With recent world-wide events, a lot of studies related to virus spreading prevention are being carried out. One of the most important topics is human body temperature monitoring. An article entitled “Investigation of the Impact of Infrared Sensors on Core Body Temperature Monitoring by Comparing Measurement Sites” (Chen *et al*., 2020) does a very good evaluation of the performance of industrial thermometers when used on different target areas, like tympanic or forehead.

The tympanic has a temperature that is very close to the core temperature of the human body (Wahyuningtya *et al*., 2023). However, measuring tympanic temperature is not an easy process, as it requires the probe to be adjusted to the shape of the ear canal. More important, in the context of facing a global pandemic of a virus with extremely high contagion rate, this accurate method is not a solution.

At the moment, forehead temperature determination through infrared thermometry (IRT) is widely used across the globe as screening of potentially infected people, as it is a convenient, non-invasive and without risk of mutual infection. It has proven its effectiveness during the severe acute respiratory syndrome (SARS) era (Perpetuini *et al*., 2021). However, IRT devices don’t exactly have a proven reliability (Yaffe, 2020). When using a noncontact IRT, (Ng *et al*., 2005) came to the conclusion that a higher temperature than 35.6 °C could be considered as fever. In another study (Ng *et al*., 2005), by comparing the relationship between facial skin temperature measured using an IRT and a direct thermometer, it was established that a safe threshold for fever would be 35.5 °C.

In Chen et al. (2020), a series of measurements are taken using two commercial and one industrial IRT. A statistical analysis is performed over the measurement data. In one experiment, the tympanic temperature in the right and left ears, the forehead temperature

and the wrist temperature of 614 randomly chosen persons was measured using a BRAUN IRT-3020 thermometer. The coefficient of variance (CV) was calculated to determine the accuracy of the measurements. The result showed a big gap of around 2.2 °C between ear temperature and forehead measurements on the same subject. In addition, it was realized that ambient temperature didn't show a very significant influence on the measured temperature.

The conclusion of the BT study is that there is a measurement uncertainty when using IRT. However, forehead IRTs are definitely suited for quick screening and recommended threshold to be used is around 36 °C.

Similarly, HR monitors have been widely used around the world. The devices allow the test subject to have a real-time measurement of their HR. The first electrocardiography (ECG) accurate wireless HR monitor was invented by Polar Electro in 1977 as a training tool for the Finnish National Cross Country Ski Team. The concept of intensity training by HR swept the athletic world in the eighties, and in 1983 which led to the introduction of the first wireless HR monitor. However, below are the summaries of some of the related works done in the past:

Gao (2003) proposed a HR monitoring system for the detection and classification of five cardiac conditions. He used signal processing techniques and Artificial Neural Network (ANN) to implement real-time processing, intelligence, cost-effectiveness and efficient use of the ECG diagnostic system. He suggested the use of remote diagnostic medical systems for diagnosing at homes for further research.

Egejuru (2008) proposed a HR monitor and arrhythmia detector which uses a low power microcontroller (MSP430FG4816) for signal analysis. The device was intended for use by medical practitioners in developing countries. The system is low cost, low power, portable, and capable of acquisition, amplification, and interpretation of physiological signals (ECG), as well as notification whenever cardiac conditions such as tachycardia and bradycardia are experienced. The focus was on creating an ECG monitoring and alert

system that detects cardiac abnormalities like tachycardia, bradycardia, etc. However, it requires expert medical practitioners to use.

From the foregoing literature and its limitations, it was decided that a BT and HR prototype be designed and developed based on the Arduino mega microcontroller board and using the IR MLX90614 and XD-58C sensors with the incorporation of an LCD readout of the measured parameters. In addition, an ESP8266 Wi-Fi module is employed to enable remote display on a PC.

2.2 Temperature Measurement

BT is a crucial parameter in healthcare diagnosis. Temperature measurement provides information about the body's internal energy, hence its regulation and control is of vital importance. Normal BT varies by person, age, activity, and time of day. The average normal BT is generally accepted as 98.6 °F (37 °C). However, some studies have shown that the 'normal' BT can have a wide range, from 36.1 °C to 37.2 °C. A temperature over 38 °C most often means one may have a fever caused by an infection or illness. The recommended BT ranges for adults is shown in Table 2.1 (Sudhindra et al., 2016).

Table 2.1: Human Body Temperature Classification

Type	Degree (Celsius)
Hypothermia (below normal)	< 35
Normothermia (normal body temperature)	36.5-37.5
Fever (Above normal)	> 37.5 or 38.3
Hyperthermia (High temperature)	>37.6 or 38.3
Hyperpyrexia (Extreme High Temperatures)	> 40 or 41.5

Source: (Sudhindra *et al*., 2016)

All objects with a temperature above absolute zero emit infrared radiation as a result of the thermal motion of their molecules. Infrared thermography (IRT) is an imaging modality that can be used to detect this radiation which is also called thermal radiation. Human skin emits infrared radiation almost like a perfect black body and thus IRT is well

suited for the measurement of skin temperature. This is due to its non-invasive nature thus providing a cost-effective alternative to the more traditional imaging modalities.

Skin temperature is a key parameter for thermal evaluations. The emissivity of human skin is 0.96 - 0.98 for IR wavelengths in the range of 2-14 μm, whereas emissivity for a perfect blackbody is 1. Hence, the thermal radiation emitted from skin represents closely the actual skin temperature. Thus, IRT is very well suited for measuring skin surface temperature. The most common factors known to affect skin temperature and indicate abnormalities are inflammation in the subcutaneous/underlying tissues and increased or decreased blood flow (Ring and Ammer, 2012). However, standardization of the imaging technique has been problematic as the normal skin surface temperature varies between individuals. Smart image processing with automatic or user-assisted recognition of regions of interest (ROI) may offer a solution to this issue. In this study, the ROI is the forehead.

2.2.1 The Physics of IR – Radiation

Electromagnetic radiation consists of oscillating electric and magnetic fields that propagate at the speed of light. The radiation has wave properties and thus it does not require a medium for propagation. Furthermore, sinusoidal electromagnetic waves are functions of time and position and they possess a definite frequency and wavelength. These waves form the electromagnetic spectrum i.e. radio and TV radiation, microwaves, IR, visible light, ultraviolet radiation, X-rays and gamma rays. As the frequency of the radiation increases, the wavelength shortens and photon energy increases as described by the equation (2.1).

$$E = hf = \frac{hc}{\lambda} \quad \text{..... 2.1}$$

where h is Planck's constant ($h = 6.626 \times 10^{-34}$Js), f is the frequency of the radiation, c is the speed of light (3×10^{8}m/s) and λ is the wavelength of the radiation (Moorthy and Sankar, 2019). In this study, the region of IR (Infrared means "below red") radiation is

the most important part of the light spectrum. IR radiation has a lower energy than visible red light. The IR spectrum ranges from 0.77 µm to 1000 µm. Furthermore, IR radiation is emitted by all objects which have a temperature above absolute zero (-273.15 °C or 0 Kelvin) as a result of the thermal motion of their molecules (Modest, 2003). The relationship between the radiated energy and temperature is described by the Stefan-Boltzmann law (2.2) (Sullivan and Edmondson, 2008):

$$E = \sigma T^4 \quad \text{....} \quad 2.2$$

where E is the total emissive power (W/m^2), σ is the Stefan Boltzmann's constant ($\sigma = 5.67 \times 10^{-8}\ W/m^2K^4$) and T is the absolute temperature (K). This equation applies only for perfect black bodies that absorb all incident electromagnetic radiation (emissivity $\varepsilon = 1$). For real objects or surfaces whose emissivity is below 1 ($\varepsilon < 1$), the following equation is used.

$$E = \sigma \varepsilon T^4 \quad \text{.....} \quad 2.3$$

where ε is the emissivity of the emitting object at a fixed wavelength (Sullivan and Edmondson, 2008). Emissivity depends on the material and surface properties. Thus, it is crucial to use the correct emissivity value which is optimized for the wavelength range in use and object being investigated (Diakides *et al.*, 2013). A perfect blackbody does not reflect or transmit any incident radiation but absorbs all of it (Meola, 2012). Moreover, emissivity depends on the viewing angle. It remains constant until approximately 50° but at greater angles, the emissivity decreases because real objects, unlike a perfect blackbody, do not emit IR radiation similarly in all directions.

To describe the emissivity of a real object (patient), a Gray body model is used. In this case the emissivity is a positive number smaller than 1. The emissivity of the surface changes and it is dependent on wavelength. The comparison of the radiance of a blackbody, gray body and a real object at a constant temperature is shown in Figure 2.1.

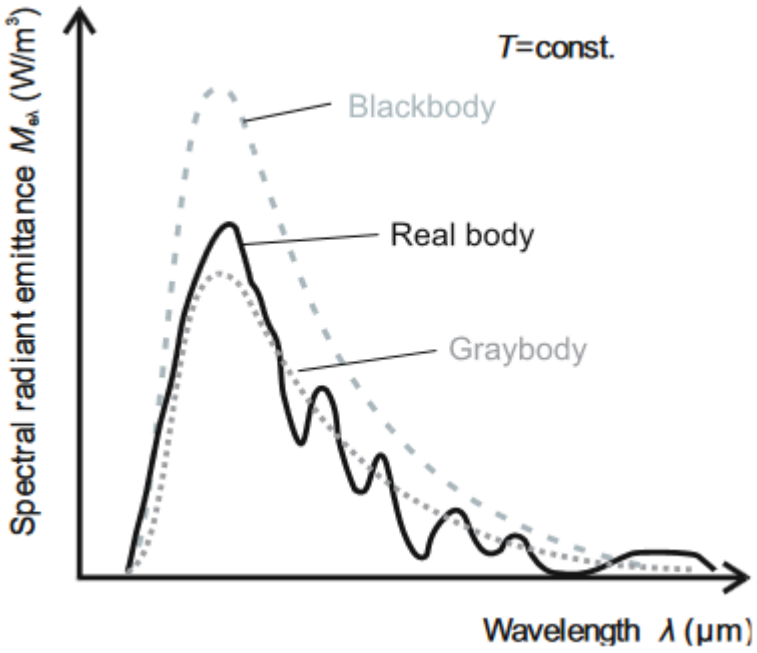

Figure 2.1: Blackbody, Graybody and Real Object Radiance

Source: (Dobesch & Poliak, 2013)

2.2.2 IRT Technology

IR detectors can be divided into two general classes of detectors: photon and thermal detectors (Dereniak and Boreman, 1996). In photon detectors, the absorbed photon energy is detected by a direct interaction of the radiation with the atomic lattice of the material. This changes resistance, inductance, voltage or currents in the photon detector. In thermal detectors, the absorbed photon energy changes the temperature of the detector and induces a change in some measurable parameter, typically resistance, which can be detected.

Photon detectors can be further divided into photoconductive and photovoltaic detectors. In photoconductive detectors, bound electrons are excited to a mobile state where they can move freely through the material. While radiation increases the number of conductive electrons, more current flows through a bias circuit. In photovoltaic detectors, the photo excited carriers are collected in a diode junction (Diakides *et al*., 2013).

In thermal detectors, the changed temperature in the detector is typically sensed by a bolometer. In a bolometer element, the resistance changes in parallel with the temperature. Furthermore, a bias circuit across the bolometer converts the changing current into a signal output (Diakides *et al*., 2013). The technological improvements in bolometers occurring in the past decade have enabled manufacturing of uncooled microbolometers that can be fabricated on top of silicon-integrated circuitry as shown in Figure 2.2. With this method, the change in resistance in each pixel in the array can be detected (Bronzino and Diakides, 2013). Furthermore, the use of uncooled microbolometers has led to reductions in both the size and the price of these types of camera.

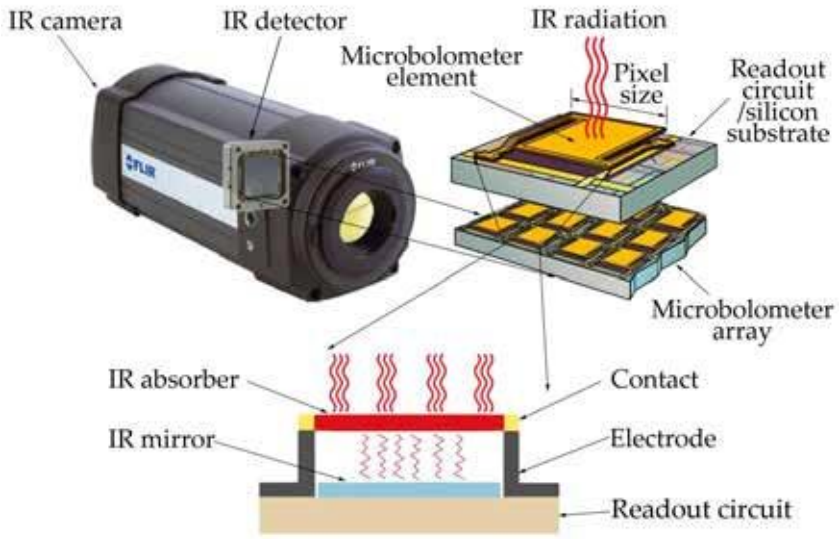

Figure 2.2: Illustration of an IR-camera Construction and Its Uncooled Microbolometer Detector

Source: (Lasanen, 2015)

2.2.3 Human Thermoregulation

The human skin has a major role in temperature regulation (thermoregulation). Skin is the largest organ in human body with an area of 1.5 – 2 m^2 (Guyton and Hall, 2011) and over 30 % of the body's temperature receptive cells are located within the skin (Gratt, 2013).

In addition to its role in thermoregulation, skin protects other organs against various injuries (mechanical stresses, electromagnetic radiation, chemicals, etc.) (Warwick and Williams, 1973). As seen in Figure 2.3, the skin consists of the epidermis and the dermis. The epidermis is an epithelial layer of the skin with no vascularity (Warwick and Williams, 1973). The thickness of epidermis varies in different parts of the body from 0.03 to 0.64 mm (Koehler et al., 2010) and it has a high capacity for regeneration after damage (Warwick and Williams, 1973). The dermis is a dense bed of vascular connective tissue which is tough, flexible and highly elastic (Warwick and Williams, 1973). Dermis contains various nervous endings and sensory receptors which help to detect pain, pressure and temperature. Furthermore, the dermis houses the sweat glands that are responsible for generating sweat and sebum (Adams *et al*., 2007). The thickness of the dermis ranges from 0.5 mm to 4.0 mm (Silver *et al*., 2001).

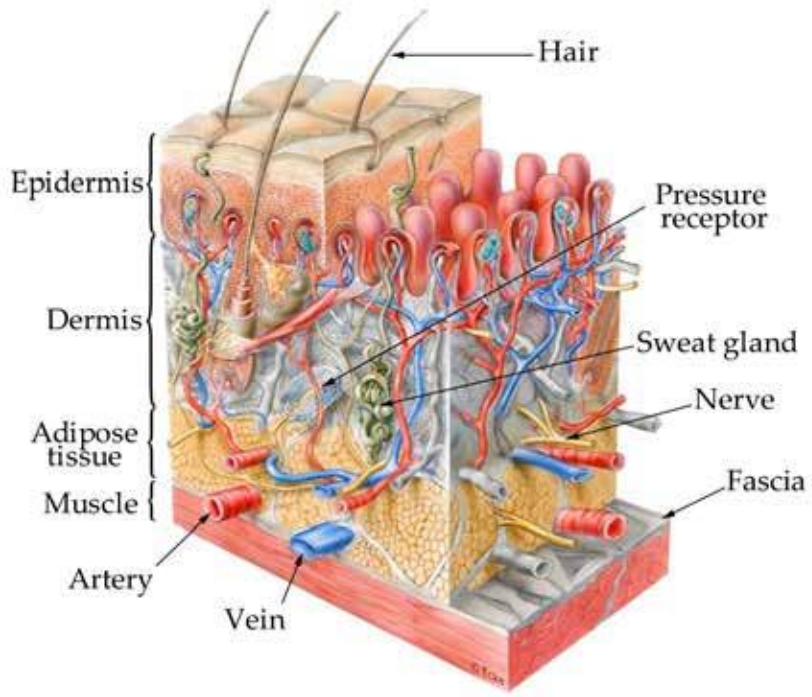

Figure 2.3: Human Skin Structure

Source: (Lasanen, 2015)

As seen in Figure 2.4, the human core temperature of a healthy individual is almost constant (within ± 0.6°C). Skin temperature can alter greatly depending on the need and extent of thermoregulation (Guyton and Hall, 2011). There are two main temperature generators in human body: digestion together with metabolism and muscle activity. The parts of the body where these mechanisms are not located, are heated by the transport of warm blood in the circulatory system. Under normal conditions, heat is transferred from the body through IR radiation (60%), thermal conduction (18%), evaporation and perspiration (22%) (Guyton and Hall, 2011). Heat is conducted into the air and may be carried away by the convection air currents.

The body temperature is controlled by nervous feedback mechanisms situated in the hypothalamus, where specialized thermoreceptor neurons monitor the blood temperature (Jones, 1998). If there is a need for loss of heat, the body starts to decrease heat production, vasodilation occurs in the skin blood vessels and perspiration is triggered. In contrast, if the body needs to increase temperature, there is an increase in thermogenesis accompanied by piloerection and vasoconstriction of blood vessels in the skin (Guyton and Hall, 2011). Vasodilation and vasoconstriction of skin blood vessels are very effective methods for temperature regulation because skin can act both as an effective heat radiator and as an insulator, depending on the amount of blood flowing through the organ (Kellogg, 2006). The nutritive blood flow needed by skin is only 0.2 mL/min (Pennes, 1998), whereas the maximum blood flow rate can be as high as 24 mL/min during heat stress (Charkoudian, 2003).

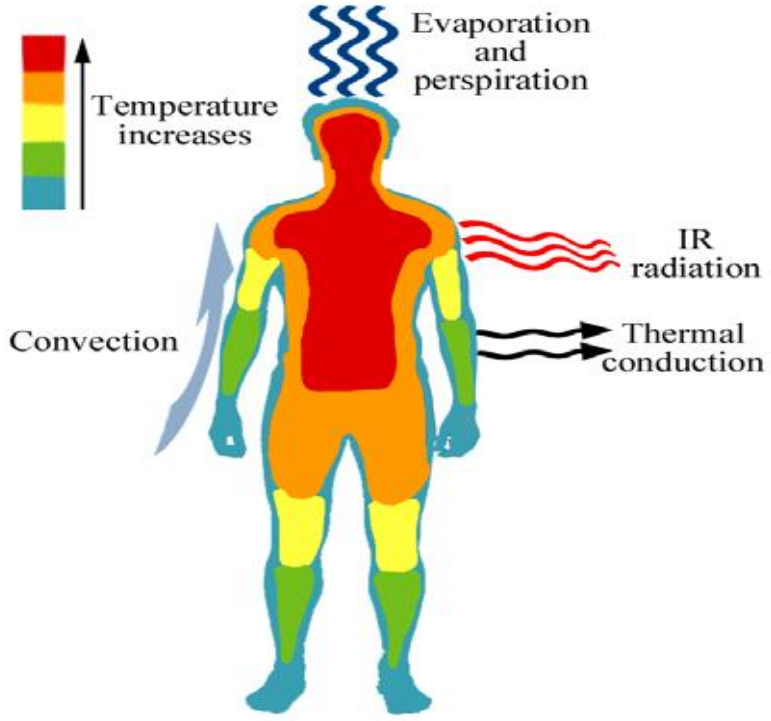

Figure 2.4: Heat Transfer Mechanisms and Temperature Distribution in Different Parts of the Body

Source: (Lasanen, 2015)

2.2.4 The MLX90614 Temperature Sensor

Temperature measurement is carried out by means of an MLX90614 sensor shown in Figure 2.5. It is built from two IC's, the IR thermopile detector MLX81101 and the Digital Signal Processor (DSP) ASSP MLX90302, specially designed to process the output of the IR thermopile output signal. It also contains a bank of digital filters. It is used because it has an inherently stable response to DC radiation, not too sensitive to ambient temperature variations, and it responds to a broad infrared spectrum which doesn't require a source of bias voltage or current (Sudianto *et al.*, 2020).

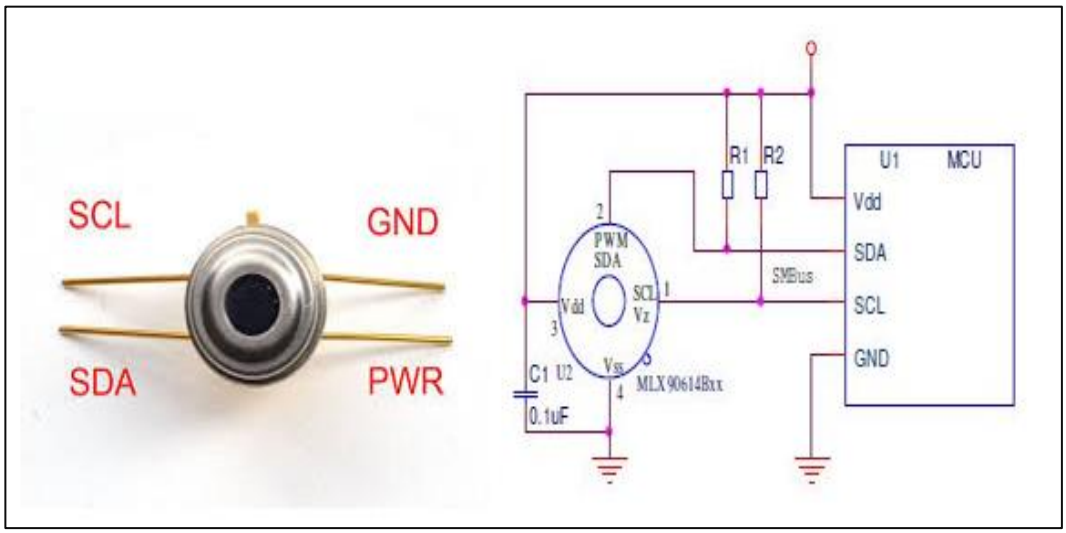

Figure 2.5: The MLX90614 Pin Description and Connection to SMBus

Source: (Sudianto *et al*., 2020).

Pin function of MLX90614 is shown in Table 2.2.

Table 2.2: Pin Functions of MLX90614

Pin Number	Pin Name	Pin Function
1	SCL	Serial Clock Input
2	PWM/SDA	Data In/Out
3	PWR/VDD	External Supply Voltage
4	GND/VSS	Ground

Source: (Jin *et al*, 2015).

The MLX90614 is factory calibrated in wide temperature ranges from -40ºC to 125ºC for the ambient temperature and -70ºC to 382.19ºC for object temperature. To perform a correct measurement, the objects frame dimension S is used and expressed as

$$S = 2 \,.\, D. \tan(\alpha) \quad \text{..... 2.4}$$

where D is distance from the target or object and ∝ is the field of view (FOV) of the sensor (Dobesch and Poliak, 2013). This is shown in Figure 2.6.

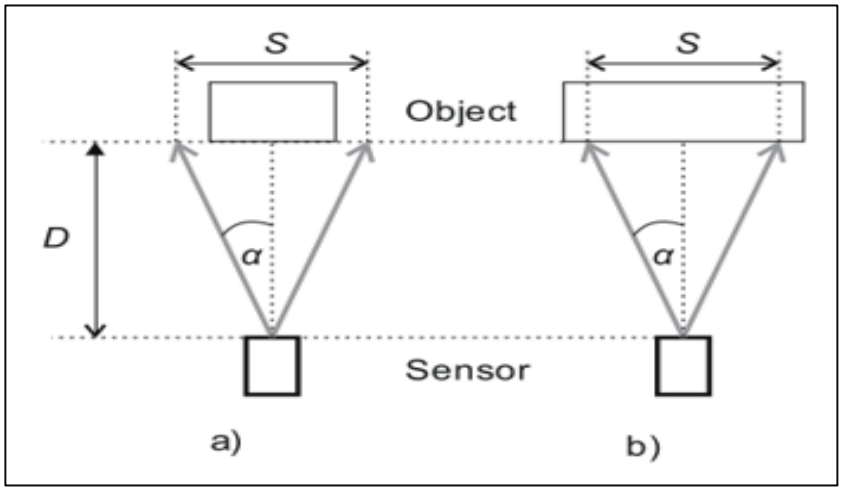

Figure 2.6: Field of View (a) Wrong and (b) Correct Measurement Setup

Source: (Dobesch & Poliak, 2013).

The sensor is manufactured in many variants of FOV. The variant with the smallest viewing angle provides 10°. To narrow the FOV of the sensor and so improve the measurement distance D, special Fresnel lenses are commonly used.

The signal conditioning ASSP MLX90302 combines a low noise programmable amplifier, a high resolution 17-bit ADC, and a powerful DSP unit. Therefore, the MLX90614DCI can be used in applications as a high accuracy and high-resolution thermometer. The operation of the signal conditioning MLX90302 is controlled by an internal state machine which controls the measurements and calculations of the object and ambient temperatures. The onboard temperature cell is the corresponding ambient temperature T_a, and the MLX81101 thermopile cell is the corresponding object temperature T_o. Both temperature measurements have a resolution of 0.02ºC. The sensor provides two methods of communication with the microcontroller; an SMBus (Signal Management Bus) protocol or a direct PWM (Pulse Width Modulation) sensor output can be used. The SMBus

protocol is preferred due to easier registry access and internal sensor setting. For the purpose of design, power, and portability the SMBus protocol is used.

2.3 Heart Rate Measurement

Measurement of HR is mostly used by medical professionals as a primary test to help in the diagnosis and tracking of cardiac conditions (Billman, 2011). HR is the number of times the heart BPM. An individual's HR depends on their age, body size, physical activity, medications, emotions and/or sleep. For adults, a normal resting HR is between 60 and 100 BPM as per WHO standard, depending on the person's physical condition with the average value usually around 72 BPM. Wide variations in this value can prove to be a significant indicator of the patient's ailments. HR's above 100 or below 55 may be fatal. For example, if the HR exceeds 100 BPM, then the condition is termed as tachycardia (Buttà et al., 2013) and the physiological reasons of its occurrence might include anxiety, stress, pregnancy, exercise, etc. Pathological reasons like fever, anaemia and heart disorder may also induce tachycardia. In some cases, tachycardia can significantly disrupt normal heart function, increasing the risk of stroke or causing sudden cardiac arrest or death. On the contrary, bradycardia is the condition when the HR drops below 60 BPM and it may be associated with ailments such as hypothyroidism. Bradycardia can be a serious problem if the heart does not pump enough oxygenated blood to the body. The recommended normal HR for adults is shown in Table 2.3.

Table 2.3: Heart Rate Range

Status	BPM
Bradycardia	< 60
Rest/Normal	60 – 100
Sleeping	40 – 50
Tachycardia	> 100

Source: (Aruna *et al*., 2016)

2.3.1 The Essential Principle of Photoplethysmography

The cardiac cycle is the sequence of events that happen between the beginning and the end of a HR. The cycle is composed of two main phases: the ventricular diastole and the ventricular systole. In the diastole (relaxation phase), the blood flows to the auricles, causing pressure to decrease in the blood vessels. In the systole (contraction phase), the blood is pumped out of the ventricles and distributed throughout the body, causing pressure to increase in the blood vessels (Sun and Thakor, 2016).

Several methods and devices perform HR measurement and heart monitoring. Electrocardiogram (ECG), analog converters and cardiofrequencimeters are the main equipment used to measure HR. Similarly, PPG is also used for measuring the HR. PPG is a non-invasive optical technique for measuring blood perfusion through tissues by the emission of light rays (Peter *et al*., 2016). PPG signal components provide valuable information about the cardiovascular system.

PPG can measure the HR, that is, the alterations of blood flow, detecting changes in the blood volume. A photo-emitter of IR light is coupled to a photo-receiver, using as the medium of light propagation the body segment in which is desired to register the plethysmographic signal. The pulsatile signal of the blood volume is detected by the photo-transistor as a modulation of the original signal of the carrier wave (Bhattacharya *et al.,* 2001).

The photoplethysmographic wave describes changes in the attenuation of light energy in its pathway when transmitted or reflected in tissues and bloodstream. This waveform is a representation of the systole and the diastole of the cardiac cycle in Figure 2.7. The signal is extracted from a healthy person.

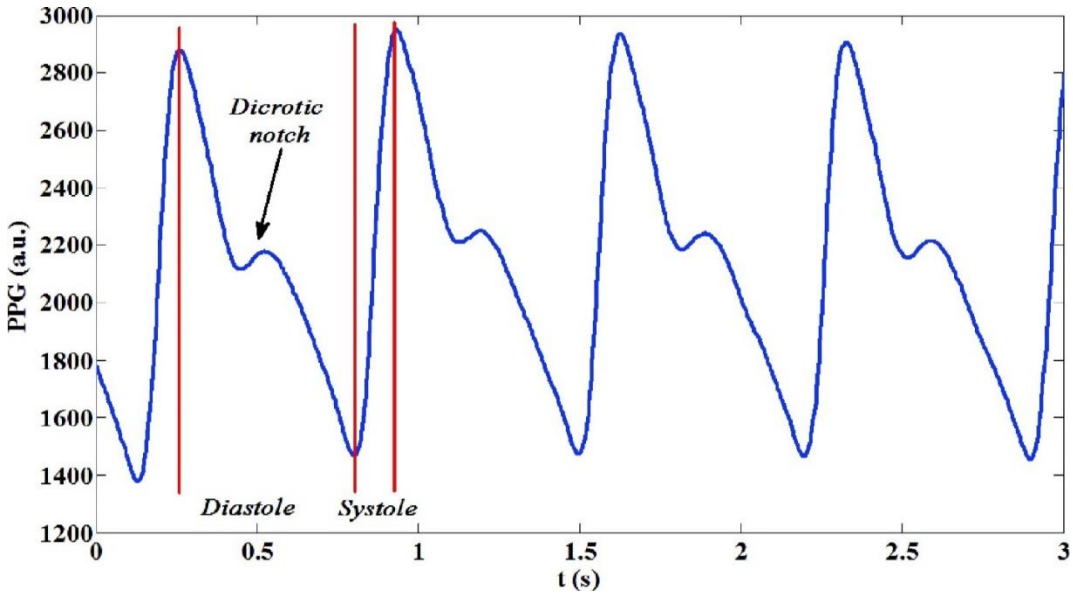

Figure 2.7: PPG Signal Waveform Analysis

Source: (Sviridova & Sakai, 2015)

The waveform of the PPG signal describes the variations in the attenuation that light energy suffers on its path when transmitted or reflected in biological tissues.

2.3.2 The XD-58C PPG Sensor

The pulse sensor amped is used for measurement of HR. It is a PPG based sensor. PPG sensors measure the amount of IR light absorbed or reflected by blood. Volume changes are caused by pressure changes in blood vessels, which occur throughout the cardiac cycle. A cardiac cycle is a sequence of events that occur between the beginning and the end of a heartbeat. There are two types of functioning principles for PPG sensors: the transmission or reflection of light through or by a certain part of the body. This is shown in Figure 2.8, the transmission operation (Figure 2.8a), in which the emission module and the photodetector are located on diametrically opposite sides; and by reflection (Figure 2.8b), in which the emission module is located on the same side as the photodetector.

With a PPG sensor in transmission mode, the LED light passes through absorbent substances, such as the skin pigmentation, bone and arterial and venous blood, and is then received by the detector (photodiode or phototransistor) for further signal processing.

In contrast, a PPG sensor in reflection mode reflects the LED light on the skin, which is received by the detector, for further signal processing. Nonetheless, this mode is applied mainly in the body parts too thick to allow the transmission of light (for instance, wrist and forehead).

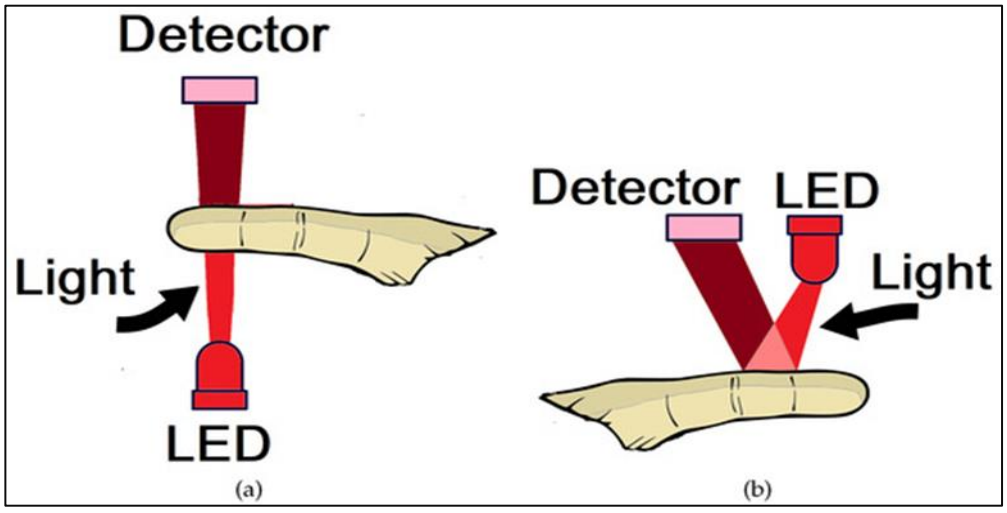

Figure 2.8: Operation of PPG Sensors for finger Application, by (a) Transmission and by (b) Reflection

Source: (Moraes *et al*., 2018)

The working principle of the PPG sensor in reflective mode is further highlighted in Figure 2.9. The results of the PPG signal depend primarily on the flow of blood and oxygen to the capillary vessels in each HR.

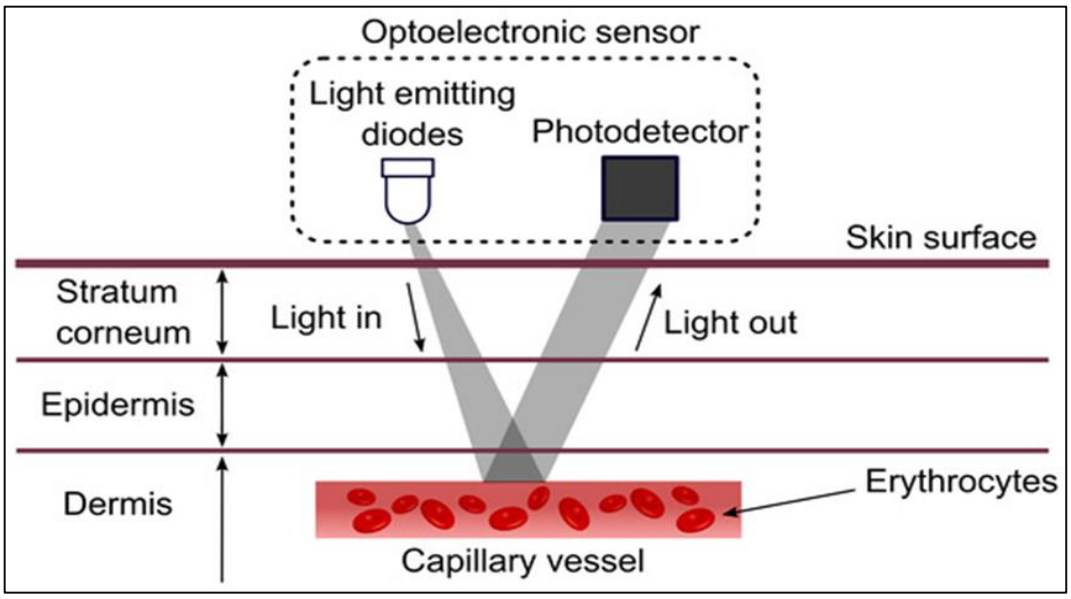

Figure 2.9: Working Principle of the Pulse Sensor Amped Reflective Type PPG Sensor

Source: (Moraes *et al*., 2018)

Theoretically, the PPG signal is formed by two components:

1. The DC offset, which represents the constant absorption of light passing through the tissues.
2. The AC component generated by heartbeats affecting blood volume when light traverses the artery.

There are several sites for measuring the PPG signal, such as the fingers and toes, forehead, wrist and ear, since all of them have a rich arterial source and are relatively easy to attach a sensor. Due to physiological particularities for each person, characteristics such as the thickness of the fat layer, rigidity of the radial artery and the skin tone have huge intervention in the morphology and amplitude of the plethysmographic wave. The Beer-Lambert law for light transmission in an absorbing medium shown in Equation (2.5) (Jayasree *et al*., 2007) relates the intensity of the emitted to the incident light, in function of light absorption by the medium, the concentration of the solution, and the path the light

travels. The higher is the luminosity emitted by the photo-emitter (LED), the higher is the amount of light transmitted through the medium as well as the amount of light reflected. Equation (2.5) is the primary basis for the functioning of the photoplethysmograph.

$$I = I_o e^{-(\mu_a d)} \quad \text{.....2.5}$$

Since blood is a highly scattering medium, the Beer-Lambert's law is modified to include an additive term G due to scattering losses and a multiplier B to account for the increased optical path length due to scattering and absorption. The modified Beer-Lambert's law which incorporates these two additions is shown in Equation (2.6) (Jayasree *et al*., 2007). The principle of operation of the XD-58C sensor is thus based on Equation (2.6).

$$I = I_o e^{-(\mu_a dB+G)} \quad \text{..... 2.6}$$

Where: I is the transmitted intensity, I_o is the input light intensity, μ_a is the absorption coefficient, d is the distance between source and detector, B is a multiplier accounting for the increased optical path length due to scattering and absorption and, G is a factor dependent upon the measurement geometry and the scattering coefficient of the tissue interrogated.

The wavelength of the source used is of significant importance in PPG. Light sources that operate in the near red (600–700 nm) and near infrared (880–940 nm) of the spectrum are most effective because whole blood has a relatively small absorption at wavelengths greater than 620 nm.

CHAPTER THREE

METHODOLOGY

3.1 Prototype System Flow Chart

Figure 3.1 shows the flow chart for the design of the prototype. It entails the processes of component installation, testing, data processing, and system analysis. The design includes hardware and software components.

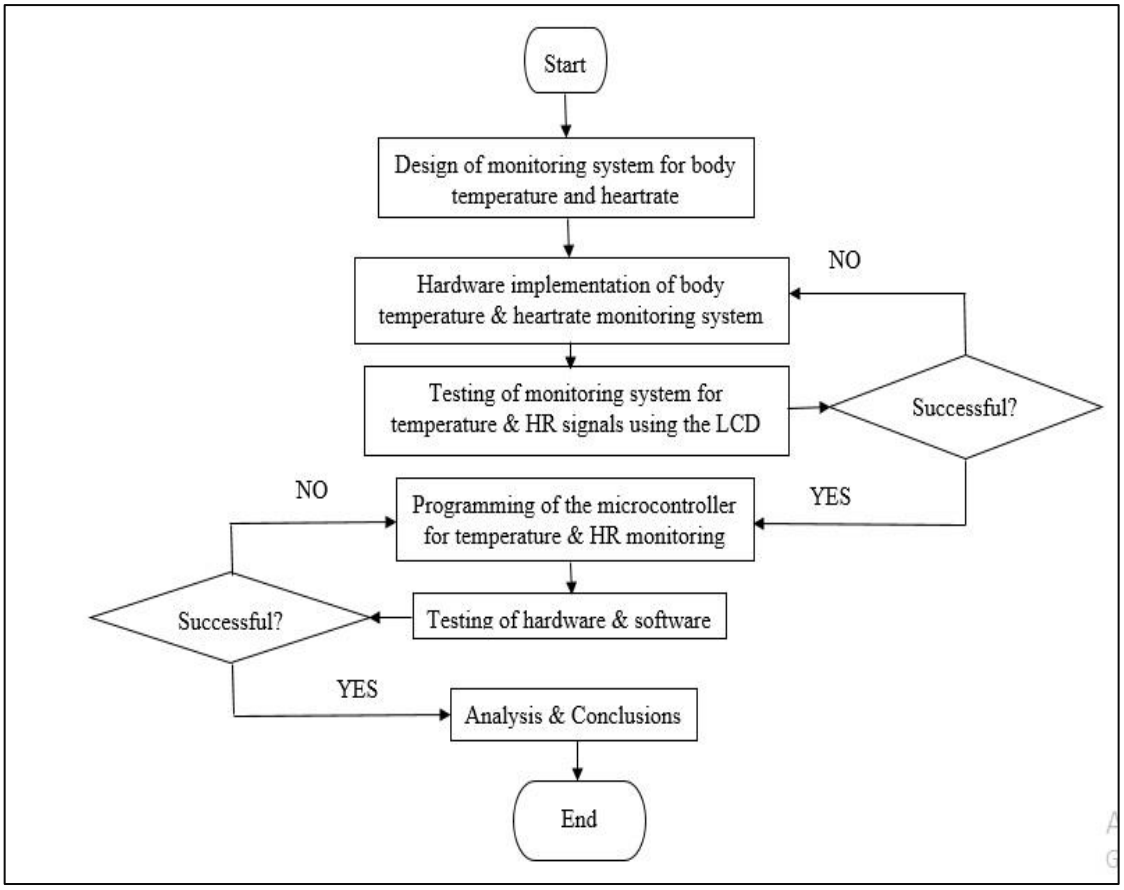

Figure 3.1: System Design Flowchart

3.2 Prototype Design and Development

A modularized approach was adopted in the design and implementation of the prototype measurement system which involves hardware and software. The hardware part consists of BT and HR sensors, the Arduino board, the LCD, a Wi-Fi module and a computer. It was divided into three major subsystems, namely; the input/output module, the microcontroller module and the transmitter/receiver module. The block diagrams of Figure 3.2 and Figure 3.3 show a general description of the prototype system.

The prototype is made up of an MLX90614 BT and XD-58C HR sensors as inputs, Arduino mega 2560 microcontroller, ESP 8266 Wi-Fi module, an LCD and a computer to display the BT and HR of patients. The BT is sensed by focusing the MLX 90614 IR sensor on the forehead of a patient. While, for measuring HR, the XD-58C IR sensor is clipped on the left-hand fingertip. Both sensors are connected to the Arduino Mega and the software ensures the sensors are functional and well-integrated. The measured parameters are then displayed on an LCD. In addition, the ESP 8266 Wi-Fi module, a microchip with TCP/IP stack and microcontroller capability allows the signals from the sensors to be transferred wirelessly to a computer or laptop for monitoring. The data is displayed using ThingSpeak API (Application Programming Interface).

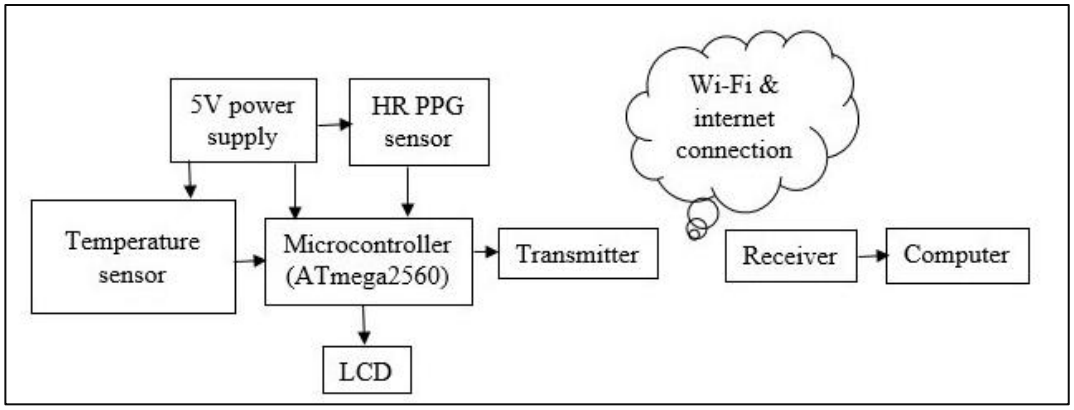

Figure 3.2: Hardware Block Diagram

The control diagram of Figure 3.3 represents the BT and HR prototype model in block diagram form. The BT and HR sensors detect the BT and HR condition of a patient and compares them with the set-point values (standard BT and HR ranges for human beings) stored in the prototype's software. A deviation of the measured values from the set-point values is an indication that the patient is sick and therefore requires the attention of the doctor. With each measurement, the output is displayed on an LCD screen and computer for continuous monitoring.

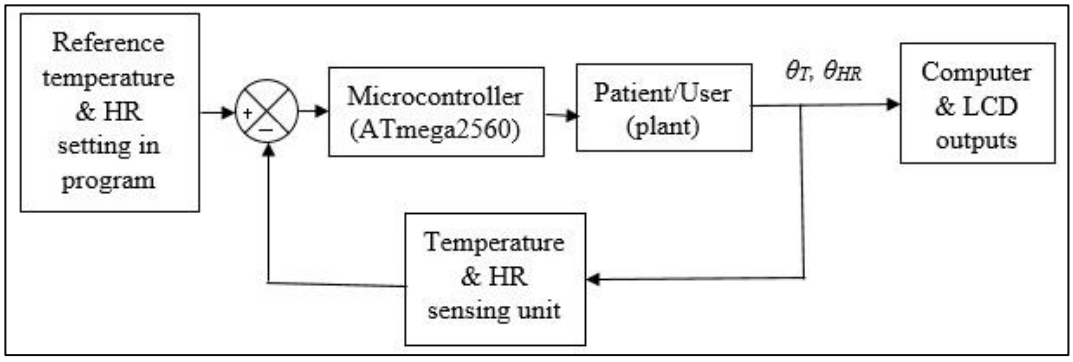

Figure 3.3: Control Block Diagram

3.3 Prototype Operating Software

The software is developed based on the Arduino module Integrated Development Environment (IDE) application with the C ++ programming language. The Arduino mega uses open-source Arduino mega IDE for compiling and uploading programs to the board. The result of program data created in the text editor (sketch) is stored in files with extension (.ino). The design begins with the creation of the MLX 90614 and the XD-58C temperature and HR sensor outputs data readings being directly sent to the Arduino in the form of input voltages. The MLX90614 output is converted from the library in the form of Fahrenheit then turned to Celsius. Similarly, the XD-58C output is converted from the library in the form of BPM. The two sensor readings are read simultaneously by the Arduino. Furthermore, the temperature sensor data and HR are stored in the database. Sensor data is displayed on the LCD on the patients end and can also be remotely sent to

the computer via the Wi-Fi connection, and SMS. Figure 3.4 shows the software design flowchart. ThingSpeak API version 1.0.2 provided the framework used to store and retrieve data from the sensors using HTTP over the internet or via local area network (LAN). A computer either a desktop or laptop, whose properties include a CORE i5 CPU, 4GB RAM and 256GB ROM is ideal for use. This is so because the prototype data is stored in the ThingSpeak cloud. The designed code running the prototype is shown in Appendix IV.

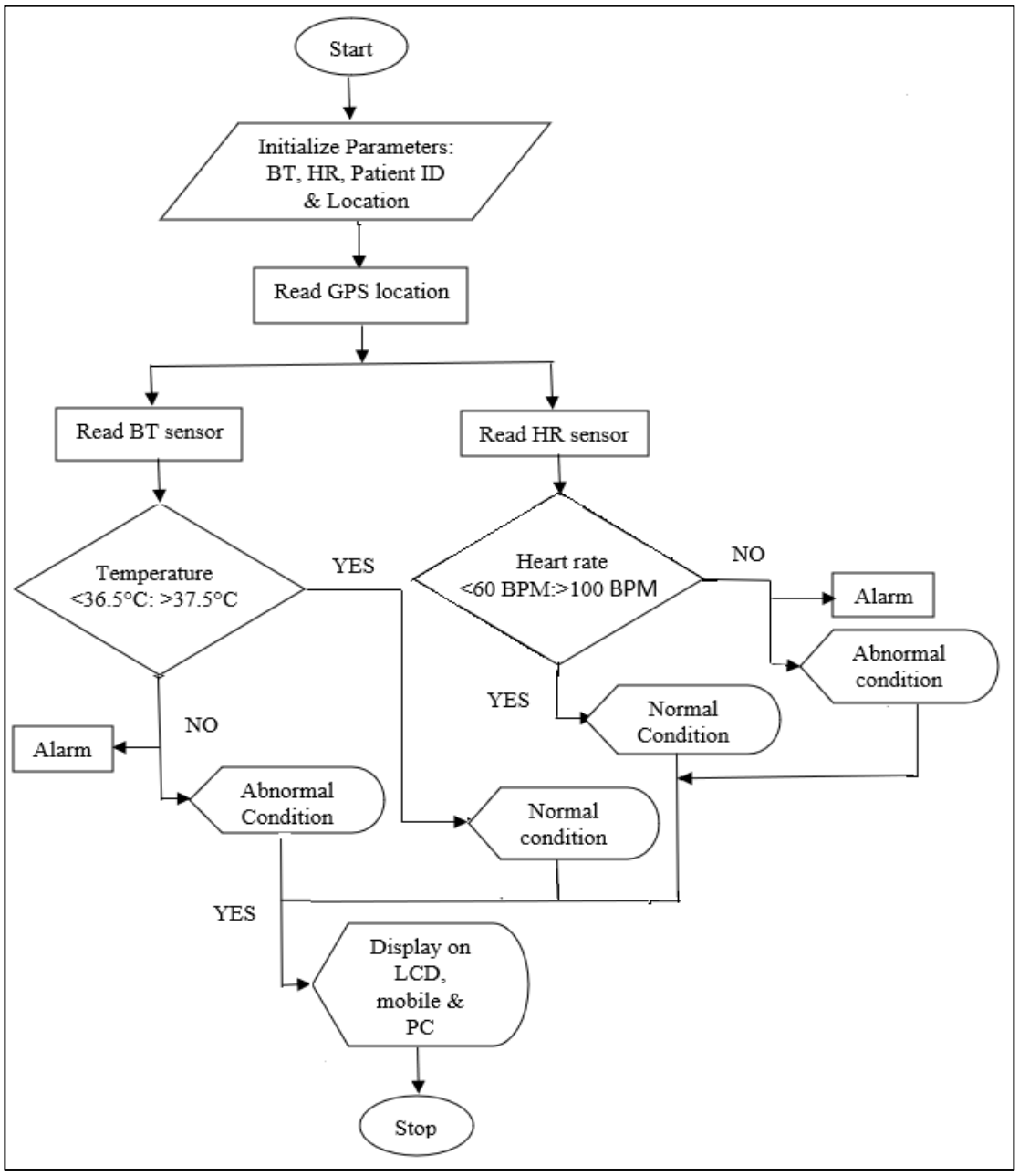

Figure 3.4: Main Program Flowchart

3.4 Circuit Diagram

The circuit diagram of the prototype system is shown in Figure 3.5. It shows the Arduino mega 2560 board and its associated pins. The Arduino Mega 2560 is a microcontroller

board based on the ATmega2560. It has 54 digital input/output pins (of which 15 can be used as Pulse Width Modulated outputs), 16 analog inputs, 4 Universal Asynchronous Receiver/Transmitter's (hardware serial ports), a 16 MHz crystal oscillator, a Universal Serial Bus (USB) connection, a power jack, an In-circuit serial programming (ICSP) header, and a reset button. The crystal oscillator is connected to pins 33 and 34 and has been used for timing the various operations of the microcontroller. The MLX90614 temperature sensor is connected to digital input pin 17 and is responsible for sensing the BT of a patient. The XD-58C PPG sensor is connected to input pin 97 and is used for the sensing of the patient HR. The Global Positioning System (GPS) module is connected to communication pins 12 and 13. The module is responsible for remotely identifying the position of the patient in the field and is useful whenever ambulatory services may be required. The Global System for Mobile Communications (GSM) module is connected on pins 45 and 46. It has been used for mobile transmission/receiving of data between the physician and the patient ends. The ESP8266 Wi-Fi module is connected to communication pins 51 and 52 and is responsible for the display of patient data on the PC. The LCD may be connected to any of the chips output pins. The SD (secure digital) module has been used as a storage device for the bulk data generated by various patients while under test. A picture of the realized prototype setup is shown in Appendix V.

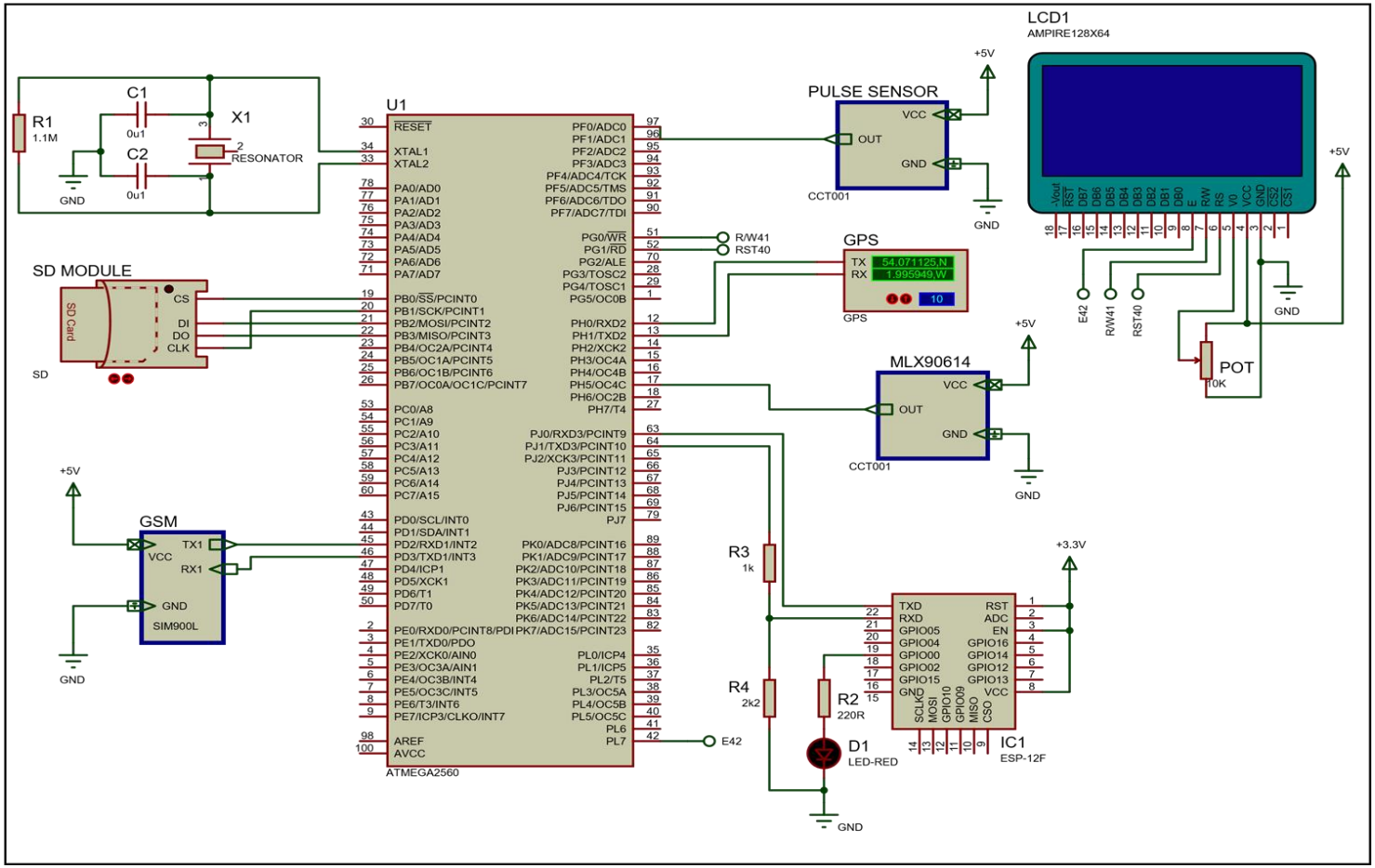

Figure 3.5: Circuit Diagram

CHAPTER FOUR

RESULT AND DISCUSSION

4.1 Experimental Conditions and Environment

Tests were carried out between the prototype and the electronic digital thermometer and sphygmomanometer as the established methods for the measurement of BT and HR respectively. This was to validate whether the two methods are in agreement with each other. The aim was to investigate this correspondence, when the BT signal is obtained from the prototype system with that obtained using the standard electronic digital thermometer. Similarly, for the sake of a suitable comparison, parallel measurements were made using a standard electronic sphygmomanometer with that of the prototype in investigating the HR signal.

The tests were done on four patients. Two signals, one for BT and the other for HR were recorded in parallel from each. The patients in the experiment were presumably healthy young or middle-aged people (3 males, 1 female; mean age: 30 years). The length of the recordings made was 20 minutes, similar to the recommended time for a standard medical examinations procedure (Musellim *et al*., 2017). The patients were asked to sit in a relaxed position and not to speak to others while the measurements were being taken to avoid collecting a lot of artifacts. Artifacts were defined as difference > 1.96 SD.

4.2 Experimental BT and HR Data Analysis of the Four Patients

In a modern clinical laboratory, it is common to have to assess the agreement between two quantitative methods of measurement. The correct approach to assess this degree of agreement is not obvious. Correlation and regression studies are frequently proposed. However, correlation studies the relationship between one variable and another, not the differences, and it is thus not recommended as a method for assessing the comparability between methods.

Bland and Altman (B&A) suggested an alternative analysis, based on the quantification of the agreement between two quantitative measurements by studying the mean difference and constructing limits of agreement (LoA). The formula for LoA is given as Equation (4.1) (Zaki, 2017).

$$\text{LoA} = \text{Mean difference} \pm 1.96 \times (\text{standard deviation of differences}) \quad \ldots\ldots\ldots\ldots \quad 4.1$$

The B&A plot analysis evaluates the bias between the mean differences, estimates an agreement interval, within which 95% of the differences of the second method, compared to the first one, fall. Data can be analyzed both as unit differences and as percentage differences plots (Giavarina, 2015). Two methods are considered in agreement if the LoA do not exceed the maximum allowed difference between methods (the differences within mean ± 1.96 SD are not clinically important) and may be used interchangeably.

The percentage difference B&A plot is specifically useful in estimating the proportional error (increase in variability of the differences as the magnitude of the measurement increases). The B&A procedure considers the proportion between the magnitude of measurements and the error graphically, but not quantitatively. That is to say that one may visualize proportional error from the B&A plot, but because the bias and repeatability estimates are computed across all of the data points, proportional error may not be apparent in the estimate. To overcome this the percentage error is determined (Hanneman, 2008).

In this study, correlation, regression and B&A techniques have been used to analyze the relationship and agreement in tests carried out by the prototype and the electronic clinical thermometer and sphygmomanometer. This was after proving the normal distribution of the data sets. MedCalc statistical software was used in constructing the scatter plots. These are shown in Figures 4.1 to 4.32 for all the four test subjects. However, due to the low sample size, the figures with correlations are more useful as illustrative than as analytic.

Error is inherent in all measurement, and consists of systematic error and random error. The bias reflects systematic error and precision (SD, confidence limits) reflect random error. Clinically acceptable bias and precision estimates of ± 0.5°C and ±0.2°C, respectively, are established a priori as the maximum parameters to indicate acceptable agreement between BT methods and precision of the difference (Janke *et al*, 2021: Ellebrecht *et al*, 2022). These limits have been used in previous studies and correspond to the usual magnitude of the human circadian temperature variation. In addition, there is an occurrence of clinical complications starting from a temperature difference greater 0.5°C. Similarly, bias and precision estimates of ±2 BPM are established as the maximum parameters to indicate acceptable agreement between HR methods and precision of the difference (Ellebrecht *et al*, 2022).

The bias and precision results are compared to the a priori specifications (Hanneman, 2008): If both fall within the set a priori criterion conditions, the new method (prototype) may be used interchangeably or out rightly replace the established thermometer and sphygmomanometer methods; If the bias exceeds the criterion, the prototype's measurements over-or underestimates the readings obtained with the thermometer and sphygmomanometer methods to an extent that would be unacceptable in practice and if the precision exceeds the criterion, the difference between the prototype and thermometer or sphygmomanometer readings is unreliable. Hence, the prototype would be an unacceptable alternative to the established thermometer or sphygmomanometer methods.

4.2.1 BT Analysis for Patient A

The data of Table 4.1 shows the BT of patient A as monitored by the prototype and the digital thermometer for a duration of 20 minutes.

Table 4.1: Body Temperature Data of Patient A as Monitored by the Two Instruments

Time (minutes)	Prototype temperature (℃)	Thermometer temperature (℃)
1.	36.59	36.6
2.	36.62	36.62
3.	36.7	36.72
4.	36.77	36.76
5.	36.79	36.8
6.	36.88	36.87
7.	36.88	36.88
8.	37	37.1
9.	37.08	37.08
10.	37.14	37.15
11.	37.29	37.29
12.	37.31	37.31
13.	37.27	37.27
14.	37.27	37.25
15.	37.31	37.3
16.	37.31	37.3
17.	37.31	37.31
18.	37.31	37.31
19.	37.31	37.3
20.	37.31	37.3

From Table 4.1 it is noted that the prototype readings (y-axis) and the thermometer readings (x-axis) are correlated by Equation (4.2) as shown in Figure 4.1.

$$y = 1.014x - 0.536 \quad \text{..... 4.2}$$

The corresponding correlation coefficient (r) is 1 and the gradient of Equation (4.2) is 1.014 denoting that there is a strong positive correlation between experimental data (prototype readings) and reference data (thermometer readings). The constant -0.536 and has units in °C and represents the core internal (homeostatic) temperature at which the body of patient A must be maintained for him to be alive.

Significance level is, $P < 0.0001$. The coefficient of determination (CoD), r^2 is 0.99 indicating that 99% of the BT readings fall within the regression line. This gives a better

goodness of fit for the measurements made by the two instruments. This in turn implies that subsequent measurements have a 99% likelihood of following this trend.

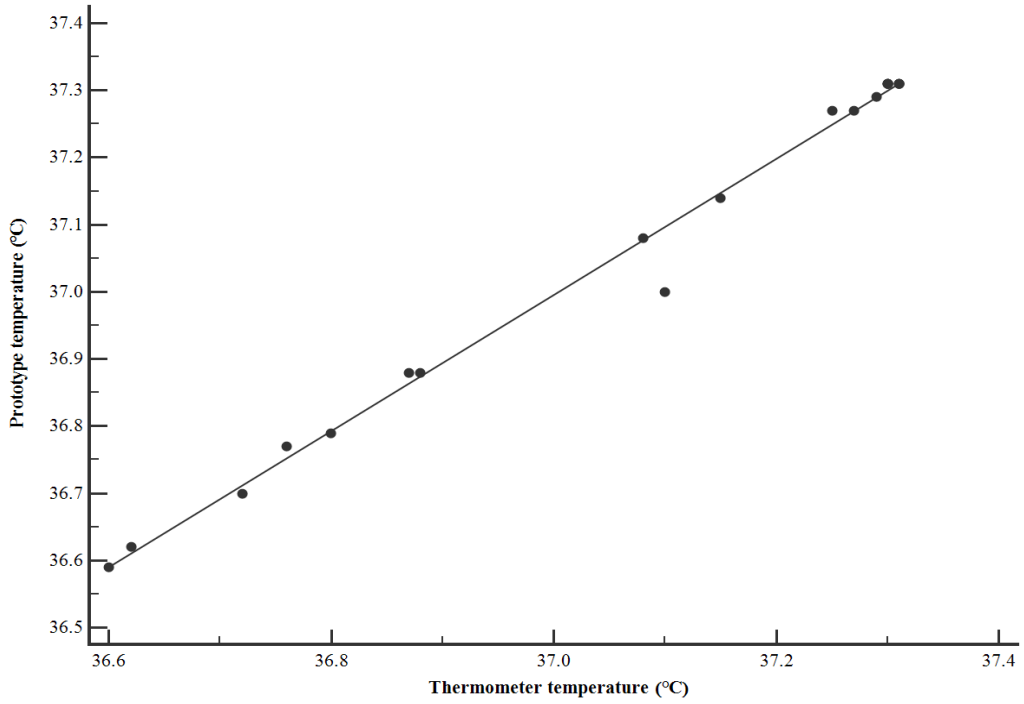

Figure 4.1: Scatter Plot of BT Monitoring of Patient A with Regression Line Indicated

From Table 4.1, the mean (±SD) BT of patient A is 37.07 (±0.27°C) and 37.08 (±0.26°C) as measured by the prototype and thermometer respectively. Thus, the mean difference is -0.0035°C. According to Equation 4.1, the LoA is -0.05 to 0.04°C. The B&A plot of the BT of patient A is shown in Figure 4.2. It can be noted that 95% of the differences are within the LoA's indicating that there is agreement between the two methods. The mean of the differences (bias) between BT as measured by the prototype and the thermometer is -0.0035°C (95% CI = -0.0149 to 0.0079). Thus, on average the prototype measured 0.0035°C less than the clinical thermometer. This bias reflects the systematic error inherent in the measurement. The error is not significant in this case because the line of equality is within the CI of the mean difference.

0.04°C (95% CI = 0.02 to 0.06) and -0.05°C (95% CI = -0.07 to -0.03) are the upper and lower LoA respectively. This indicates that the readings made by the prototype may be 0.05°C below or 0.04°C above those measured by the thermometer. In other words, 95% of the differences between the two measurement methods are within the range specified by Equation (4.3).

$$\text{Confidence limits} = \text{Upper LoA} - \text{Lower LoA} \quad \text{..... 4.3}$$

$$= 0.04 - (-0.05)$$

$$= 0.09°C.$$

The 0.09°C LoA does not exceed the priori criterion (clinically acceptable precision) of 0.2°C. Therefore, the repeatability of the prototype in monitoring BT is acceptable. The prototype is thus equivalent to the thermometer in its operation. Only a single outlier is present. This may be attributed to a possible error in the estimate due to sampling error.

$$\text{Percentage error} = \frac{\text{CI}}{\text{Mean value of clinical thermometer measurements}} \text{ x } 100 \quad \text{..... 4.4}$$

$$= \frac{0.04 - (-0.05)}{37.08} \text{ x } 100$$

$$= 0.24\%.$$

Temperature differences are scattered around the bias, with some level of a straight-line pattern (variability). This is validated by the presence of the percentage error.

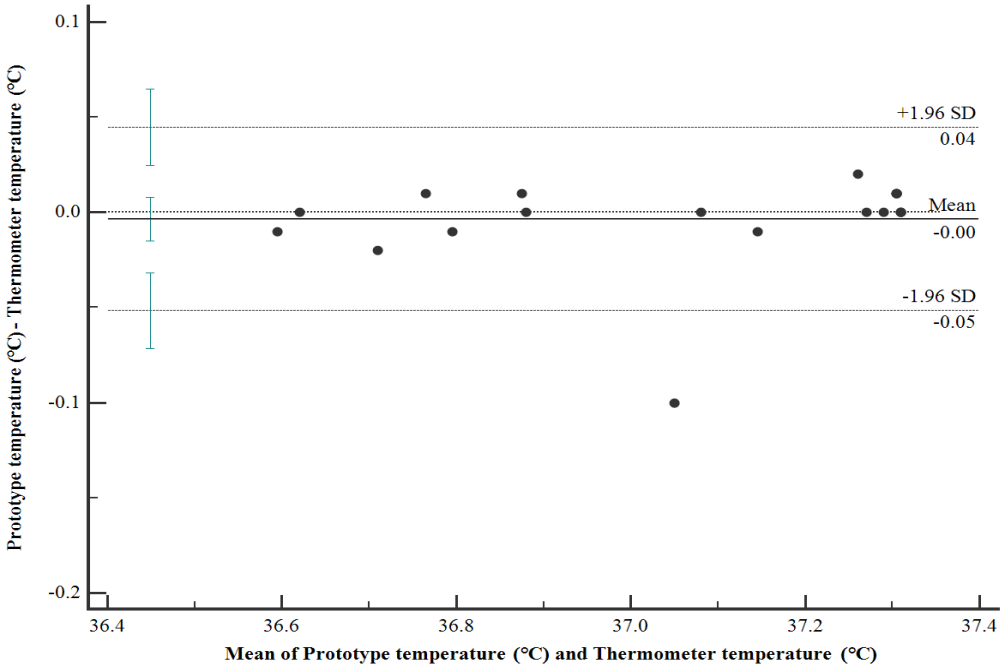

Figure 4.2: Bland-Altman BT Plot of Patient A in °C

Figure 4.3 represents the B&A percentage plot of the data of Table 4.1. The bias is -0.01%, with a constant variability across all the readings just as in Figure 4.2. The agreement limits are from -0.14% to 0.12%.

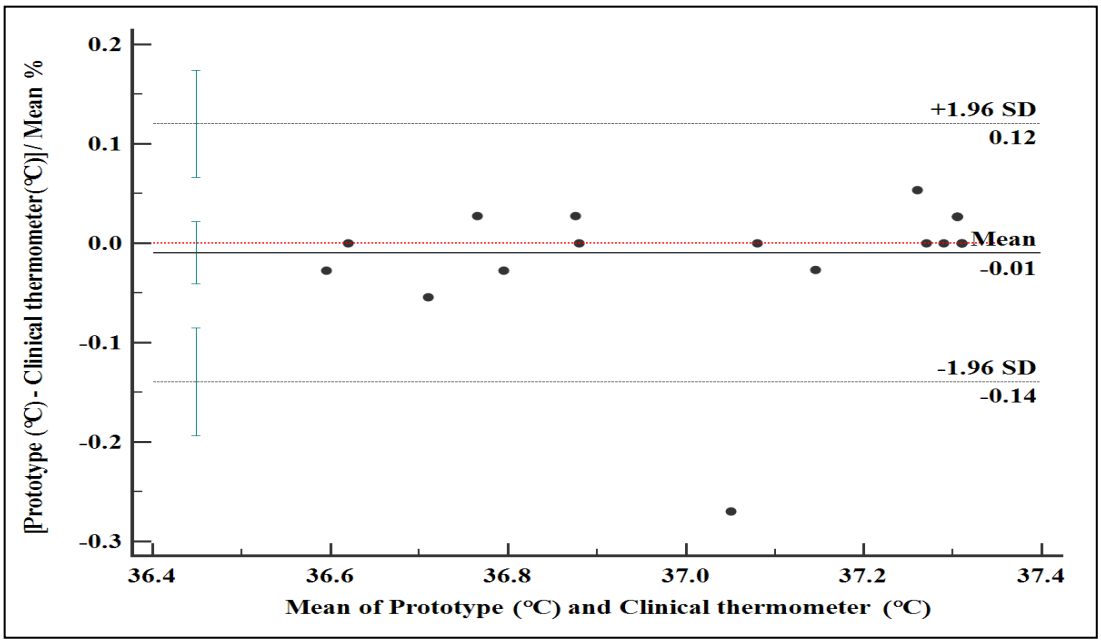

Figure 4.3: Bland-Altman BT Plot of Patient A as a Percentage

A plot of the BT of patient A as recorded by the prototype and the thermometer over a period of 20 minutes is shown in Figure 4.4. It is observed that the BT of patient A was within the desired normal of 36.5°C to 37.2°C throughout the testing. The fluctuated points along the graph are due to a combination of factors such as stress levels, anxiety, changes in ambient temperature, age, etc. for which I had no control over.

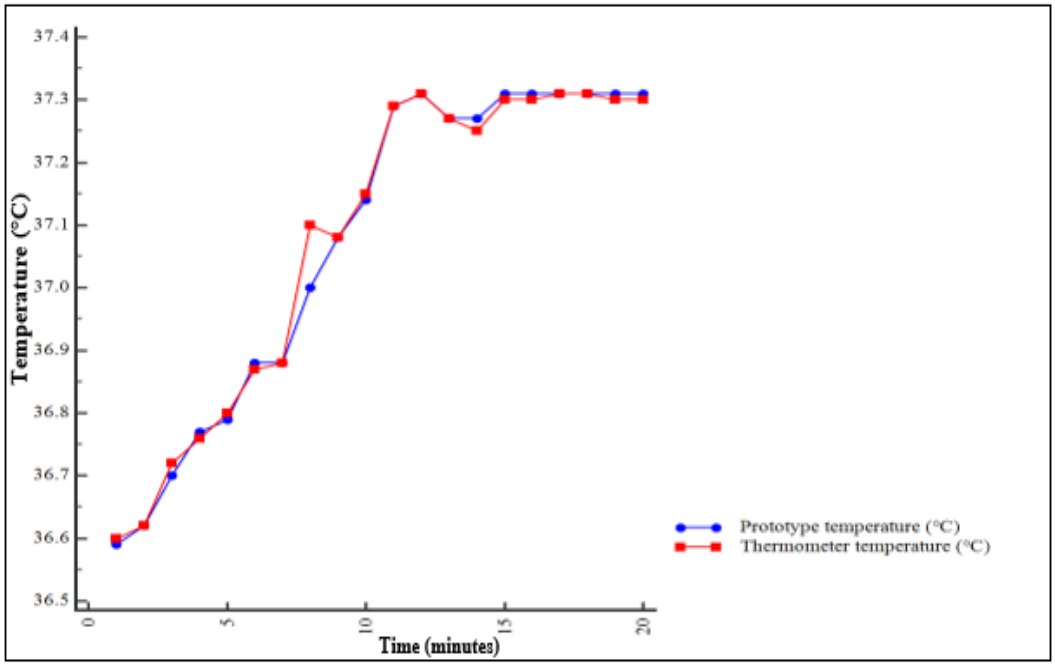

Figure 4.4: Temperature Profile for Patient A Monitored for 20 Minutes

4.2.2 HR Analysis for Patient A

Table 4.2 summarizes the HR of patient A as monitored by the prototype and sphygmomanometer measuring instruments for 20 minutes.

Table 4.2: Heart Rate Data of Patient A as Monitored by the Two Instruments

Time (minutes)	Prototype heart rate (BPM)	Sphygmomanometer heart rate (BPM)
1.	89	88
2.	67	70
3.	91	91
4.	86	85
5.	85	85
6.	96	95
7.	81	78
8.	89	88
9.	94	93
10.	85	85
11.	74	77
12.	94	94
13.	95	95
14.	91	91
15.	60	58
16.	86	87
17.	97	96
18.	83	84
19.	96	96
20.	97	97

It can be deduced from Table 4.2 that there is a straight line relation between the HR readings as measured by the two instruments. This is given by Equation (4.5) and shown in Figure 4.5.

$$y = 1.013x - 0.936 \quad \text{..... 4.5}$$

The correlation coefficient (r) is 0.99 and the gradient of Equation (4.5) is 1.013. This informs that there is a strong positive correlation between experimental data (prototype readings) and reference data (sphygmomanometer readings).

The constant -0.936 has units in BPM and defines a specific HR at which the heart of patient A must pulsate for him to be alive.

Significance level is, $P < 0.001$. The CoD (r^2) is 0.98 indicating that 98% of HR readings for patient A fall within the regression line. This shows that there is a better goodness of fit for the readings made with the two instruments. This in turn implies that subsequent measurements have a 98% likelihood of following the same trend and hence a good measure of the accuracy of the prototype in monitoring HR.

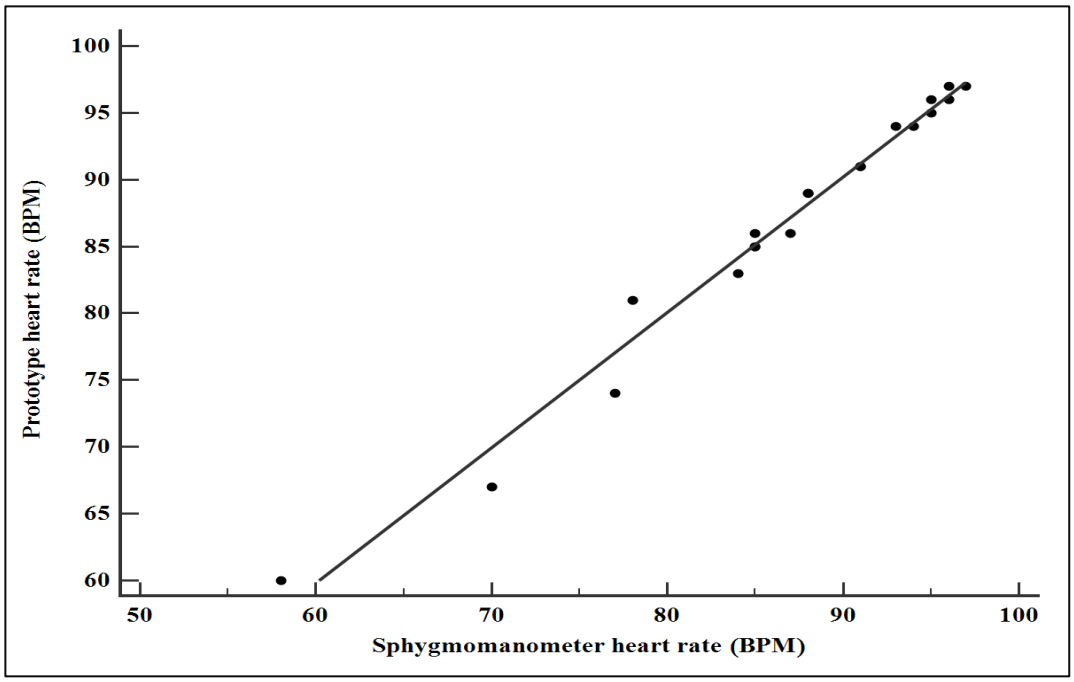

Figure 4.5: Scatter Plot of HR Monitoring of Patient A with Regression Line Indicated

From the data of Table 4.2 it is observed that the mean (±SD) HR of patient A is 86.8 (±10 BPM) and 86.65 (±10 BPM) as measured by the prototype and sphygmomanometer respectively. The B&A HR plot of patient A is shown in Figure 4.6. The bias (mean difference) between HR as measured by the prototype and the sphygmomanometer is 0.2 BPM (95% CI = -0.5 to 0.8). Thus, on average the prototype measured 0.2 BPM higher than the sphygmomanometer. A systematic error of 0.2 BPM is present in the measurement. The error is not significant as the line of equality is within the CI of the mean difference.

2.9 BPM (95% CI = 1.8 to 4.1) and -2.6 BPM (95% CI = -3.8 to -1.5) are the upper and lower LoA respectively. This indicates that the results measured by the prototype may be 2.6 BPM below or 2.9 BPM above those measured by the sphygmomanometer. 95% of the differences between these two monitoring methods are within this range. From Equation (4.2), the LoA is calculated to be 5.5 BPM. The LoA slightly exceed the priori criterion of 5 BPM by 0.5 BPM. This may be attributed to the inherent measurement error of the system. Therefore, the repeatability of the prototype in monitoring HR of patients is acceptable. Hence the prototype is equivalent to the sphygmomanometer and can be used interchangebly. Two outliers are detected. They may be as a result of a possible error in the estimate due to sampling.

$$\text{Percentage error} = \frac{\text{CI}}{\text{Mean value of sphygmomanometer measuremets}} \text{ x } 100 \quad \ldots\ldots\ldots\ldots\ldots\ldots \text{ 4.6}$$

$$= \frac{2.9 - (-2.6)}{86.65} \text{ x } 100$$

$$= 6.35\%.$$

The HR differences are scattered around the bias, with some form of a straight-line pattern (variability). This is validated by a percentage error of 6.35%.

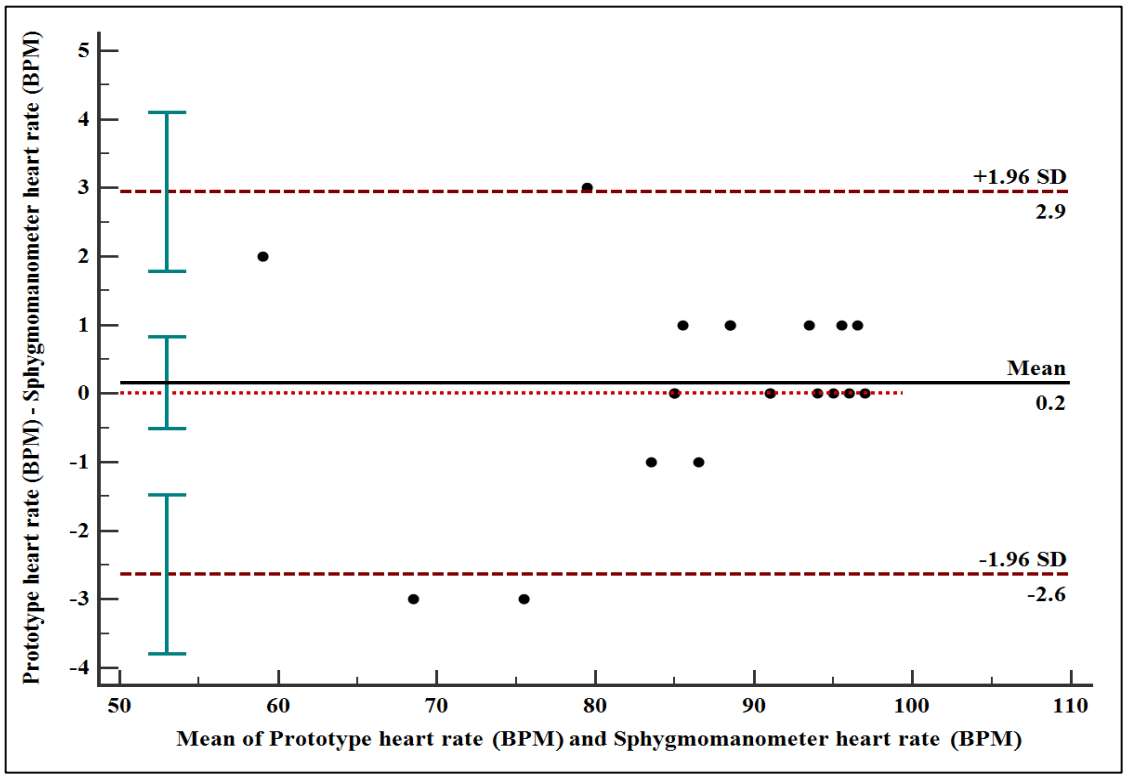

Figure 4.6: Bland-Altman HR Plot of Patient A in BPM

Figure 4.7 shows the B&A HR percentage plot of the data set in Table 4.2. The bias is 0.2% with varying and almost constant variability across all the readings, with the exception of very low measurements where there were no readings made as the patient is considered to be healthy. The agreement limits are from -3.6% to 3.9%.

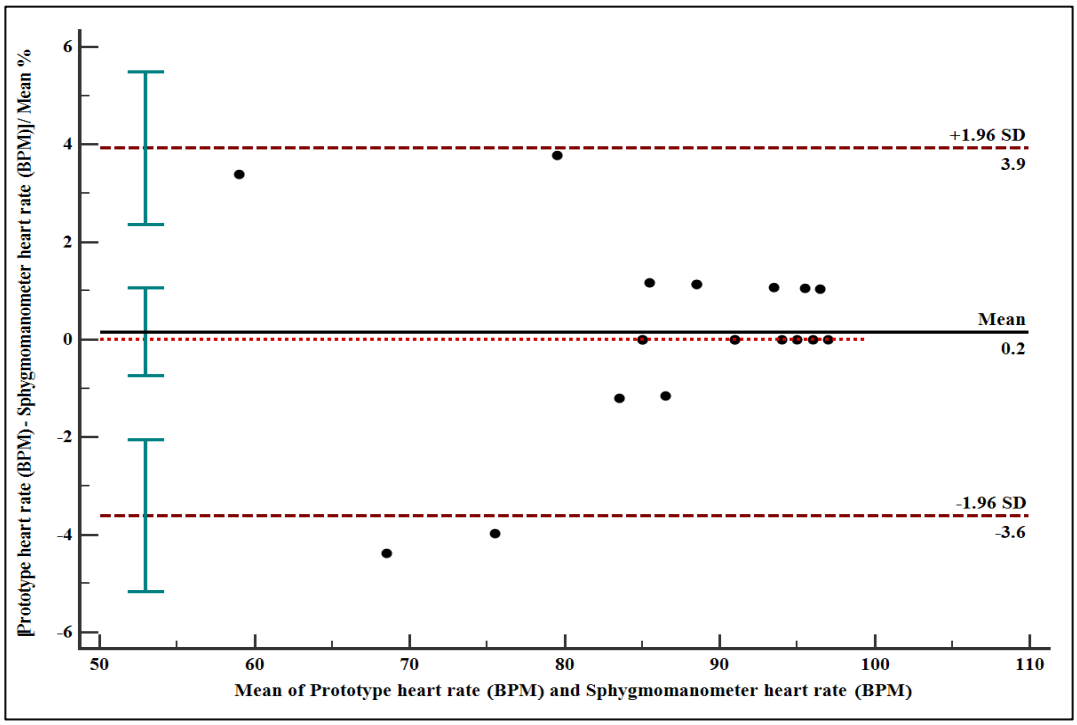

Figure 4.7: Bland-Altman HR Plot of Patient A as a Percentage

Figure 4.8 shows sphygmomanometer versus prototype HR measurements for patient A monitored for 20 minutes. The readings were in normal condition range of 60 to 100 BPM throughout the testing except for the 58 BPM bradycardic condition for the sphygmomanometer test. This may be attributed to the inherent error present in all measurement systems. The fluctuated points along the graph are due to the patient moving their finger in which the finger was not properly placed onto the detector of the sensor. Other reasons include anxiety and stress levels for which I had no control over.

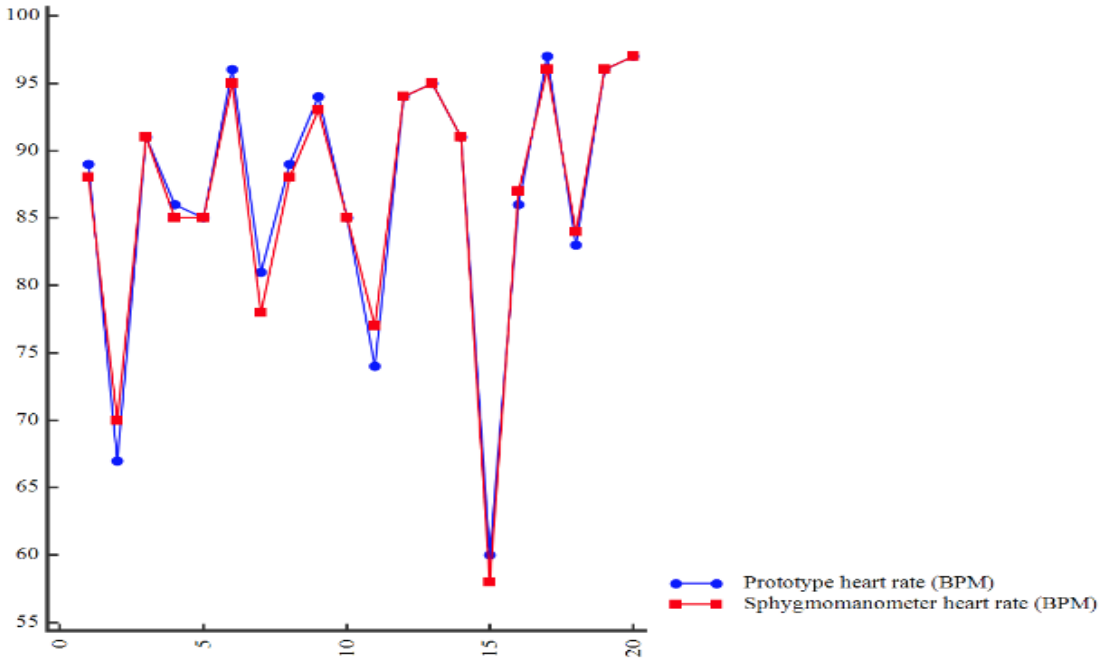

Figure 4.8: Heart Rate Profile for Patient A Monitored for 20 Minutes

4.2.3 BT Analysis for Patient B

The result obtained from monitoring the BT of patient B for 20 minutes with the two measuring instruments is shown in Table 4.3.

Table 4.3: Body Temperature Data of Patient B as Monitored by the Two Systems

Time (minutes)	Prototype temperature (◦C)	Thermometer temperature (°C)
1.	36.61	36.6
2.	36.7	36.7
3.	36.74	36.72
4.	36.8	36.81
5.	36.8	36.8
6.	37	37.1
7.	37	37.1
8.	37.08	36.87
9.	37.15	37.15
10.	37.21	37.2
11.	37.3	37.32
12.	37.34	37.32
13.	37.29	37.28
14.	37.31	37.31
15.	37.19	37.2
16.	37.38	37.38
17.	37.45	37.45
18.	37.5	37.5
19.	37.35	37.36
20.	37	37.1

The scatter plot of Figure 4.9 shows a linear positive relation between the two methods of Table 4.3 in monitoring the BT of patient B. This is given by a correlation coefficient (r) of 0.97. The measurements are related by Equation (4.7).

$$y = 0.959x + 1.528 \quad \text{..... 4.7}$$

The gradient of Equation (4.7) is 0.959 indicating the presence of a strong positive correlation between readings of the two measuring instruments. The constant 1.528 and has units in °C and it defines the core internal temperature at which the body of patient B must be maintained for him to remain alive.

Significance level is, $P < 0.0001$. The CoD (r^2) is 0.95 indicating that 95% of the BT readings of patient B fall within the regression line. This provides a better goodness of fit for the measurements made by the two instruments. This in turn implies that subsequent

measurements have a 95% likelihood of following similar trend thus providing a good measure of the accuracy of the prototype in monitoring BT.

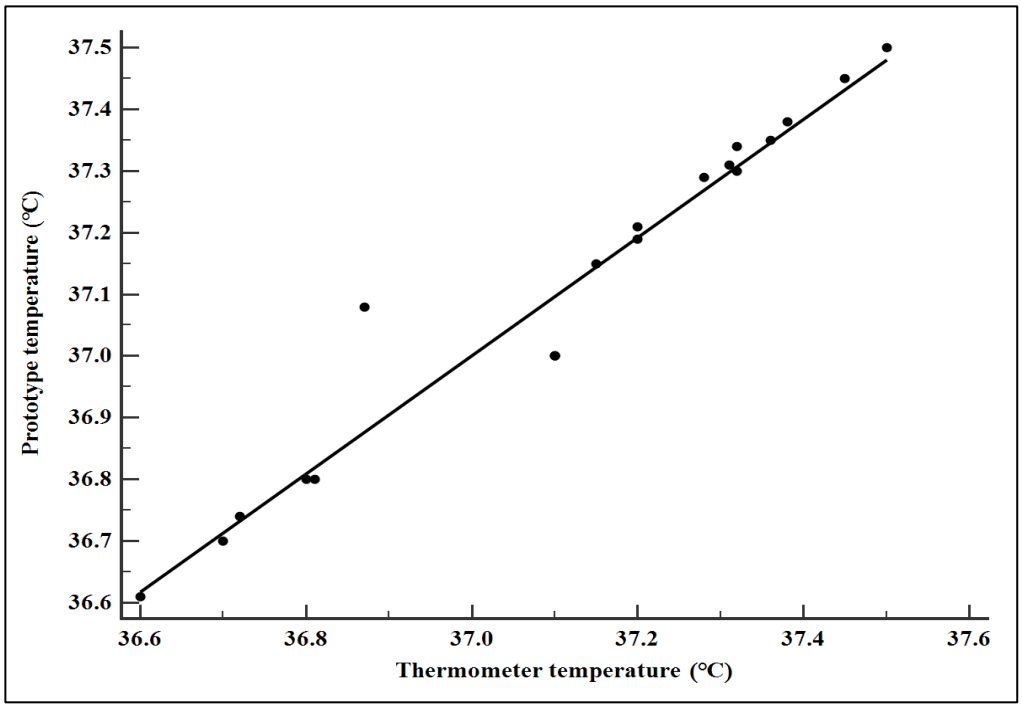

Figure 4.9: Scatter Plot of BT Monitoring of Patient B with Regression Line Indicated

The mean (±SD) BT of patient B was 37.11 (±0.27°C) as measured by the prototype and thermometer respectively from the data in Table 4.3. The B&A plot of Figure 4.10 reveals that there is a bias of -0.0035℃ (95% CI = -0.033 to 0.026) between the two instruments in reading the BT of patient B. On average the prototype measured 0.0035℃ less than the thermometer. The -0.0035℃ systematic error is not significant as the line of equality is within the CI of the mean difference.

0.12 ℃ (95% CI = 0.07 to 0.17) and -0.13 ℃ (95% CI = -0.18 to -0.08) are the upper and lower LoA respectively. This is an indication that the results measured by the prototype are 0.13℃ below or 0.12℃ above those measured by the thermometer. This is to say that 95% of the differences between the two measuring instruments are within this range. From

Equation (4.3), the LoA is found to be 0.25°C. The LoA slightly exceed the priori criterion of 0.2°C by 0.05°C. This may be attributed to the inherent measurement error of the system.

As a result, it is concluded that the repeatability of the prototype in monitoring the BT of any patient is acceptable. Only a single outlier is present. It may be attributed to a possible error in the estimate due to sampling. From Equation (4.4), the percentage error is 0.67%. The temperature differences are scattered around the bias, with some level of a straight-line pattern (variability). This is true cause of the presence of a percentage error.

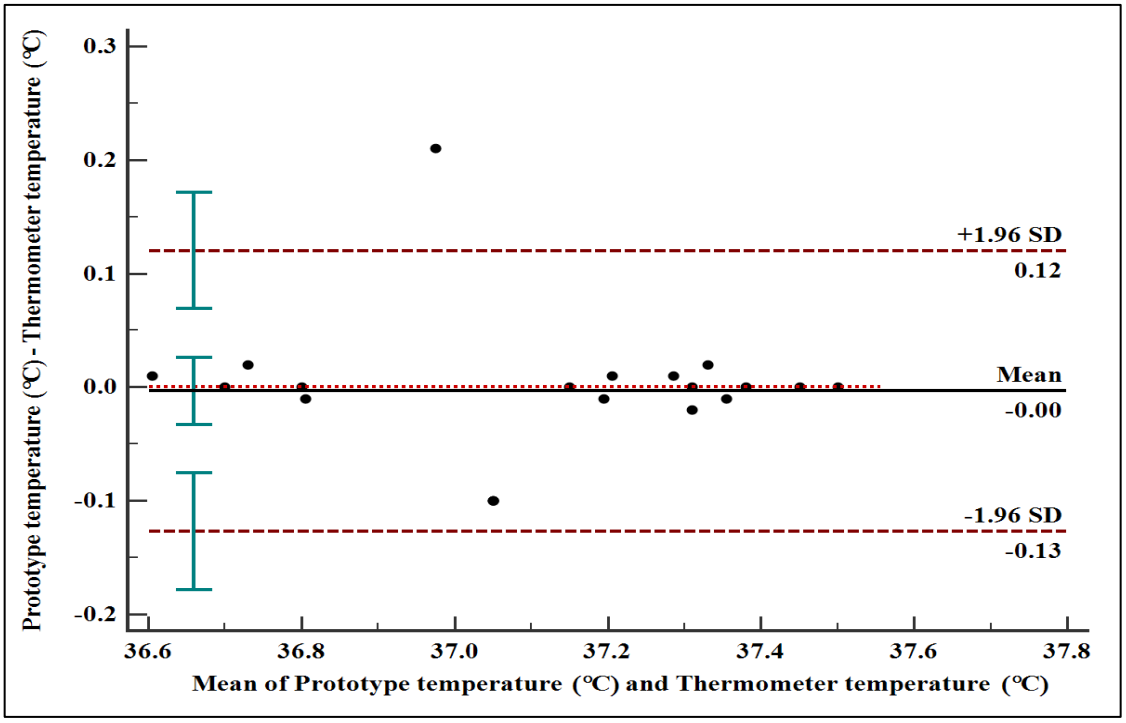

Figure 4.10: Bland-Altman BT Plot of Patient B in °C

From Figure 4.11 it can similarly be deduced that there is varying variability across all the measurements. However, this variability is almost constant with BT readings within the CI of the bias. The agreement limits are from -0.34% to 0.32%.

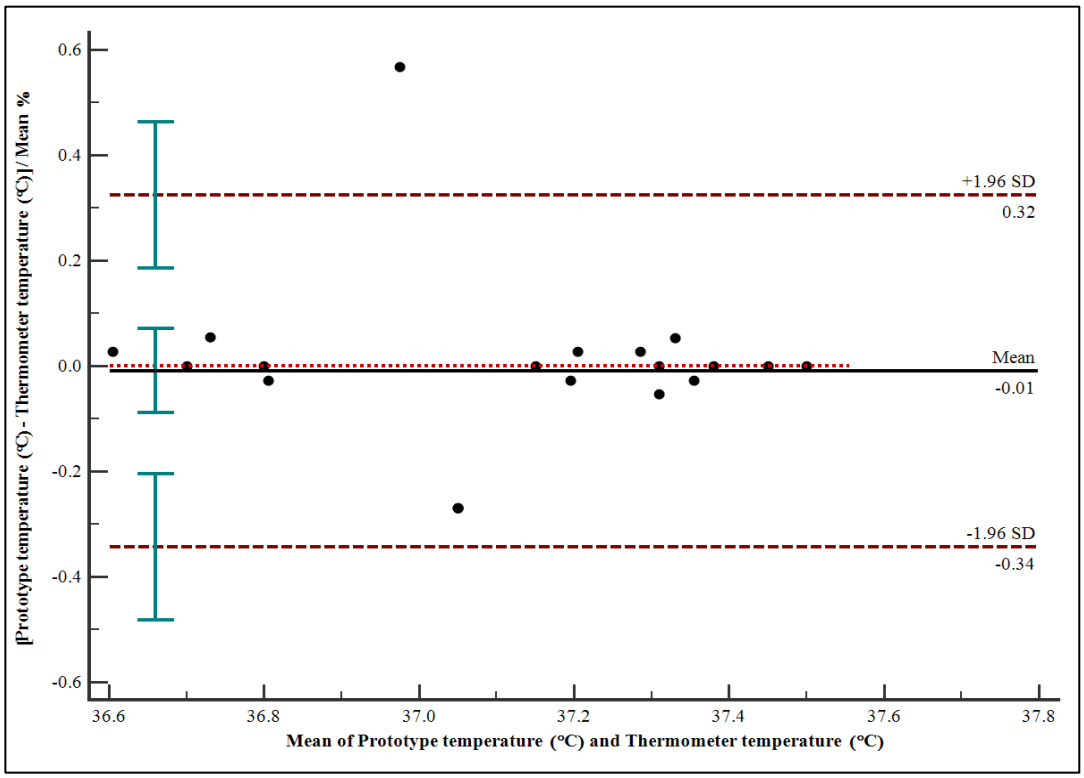

Figure 4.11: Bland-Altman BT Plot of Patient B as a Percentage

Figure 4.12 shows the thermometer BT readings against those of the prototype for patient B as captured in Table 4.3 for a time period of 20 minutes. The measurements show a normal BT condition (36.5°C to 37.2°C) for patient B throughout the experiment. The fluctuated points along the graph are due to a combination of factors similar to those of patient A.

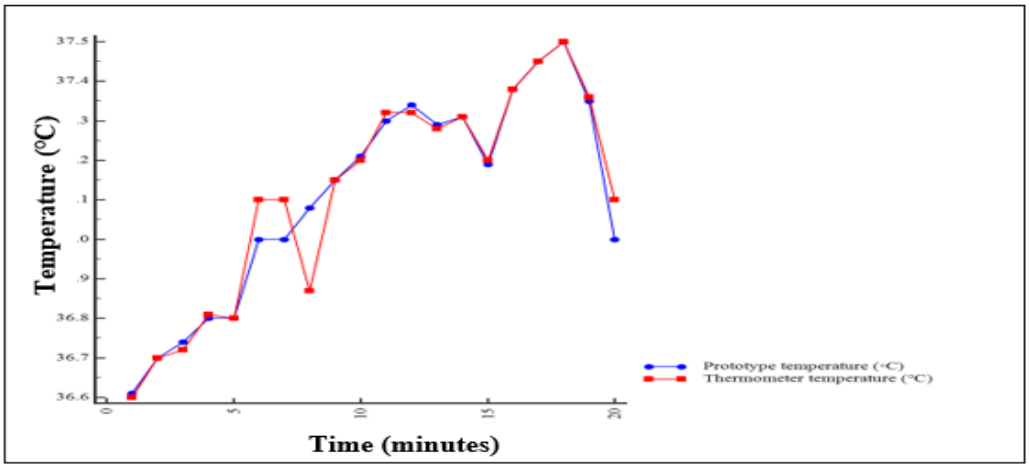

Figure 4.12: Temperature for Patient B Monitored for 20 Minutes

4.2.4 HR analysis for patient B

Table 4.4 outlines the HR data of patient B as captured by the two instruments for a period of 20 minutes.

Table 4.4: Heart Rate Data of Patient B as Monitored by the Two Systems

Time (minutes)	Prototype heart rate (BPM)	Sphygmomanometer heart rate (BPM)
1.	70	69
2.	71	71
3.	76	74
4.	80	80
5.	84	84
6.	85	86
7.	89	90
8.	84	83
9.	87	86
10.	85	85
11.	96	96
12.	72	72
13.	76	75
14.	79	78
15.	77	77
16.	75	75

Time (minutes)	Prototype heart rate (BPM)	Sphygmomanometer heart rate (BPM)
17.	77	76
18.	87	89
19.	85	87
20.	98	97

A plot of the data in Table 4.4 reveals that a linear positive relation exists between the readings of the two instruments. This is supported by a correlation coefficient (r) of 0.99 and Equation (4.8) as shown in Figure 4.13.

$$y = 0.951x + 4.149 \quad \text{..... 4.8}$$

The gradient of Equation (4.8) is 0.951 implying that there is a strong positive correlation between prototype readings and those of the sphygmomanometer. The constant of 4.149 BPM defines a particular HR at which the heart of patient B must beat for him to remain alive.

Significance level is, $P < 0.001$. The CoD (r^2) is 0.98 indicating that 98% of HR readings of patient B fall within the regression line. This tells of a better goodness of fit for the measurements made by the two instruments. This in turn implies that subsequent readings have a 98% likelihood of following the same trend as this, thus providing a good measure of the accuracy of the prototype system in monitoring HR.

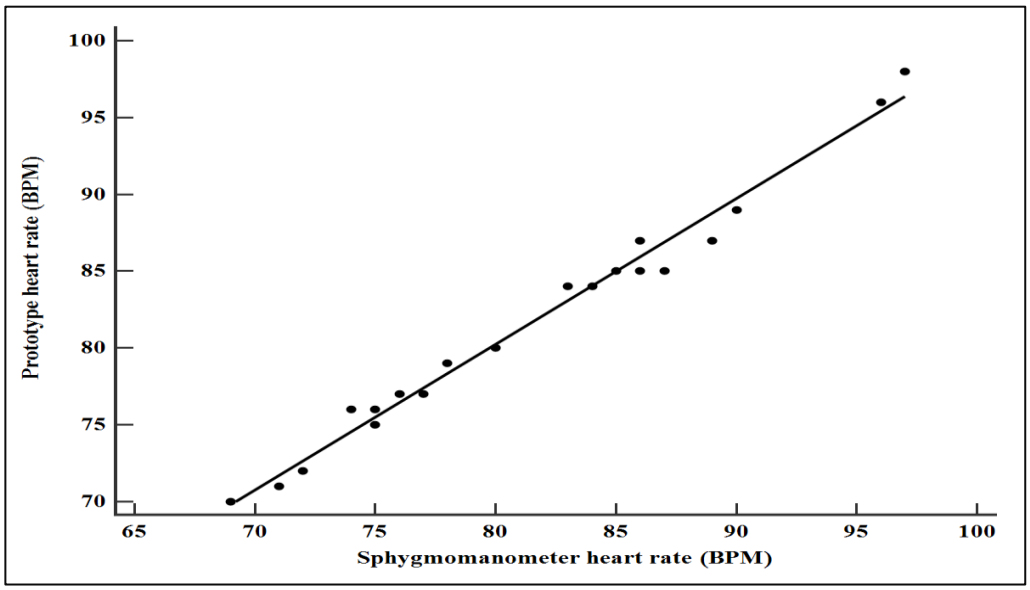

Figure 4.13: Scatter Plot of HR Monitoring for Patient B with Regression Line Indicated

Table 4.4 gives the mean (±SD) HR of patient B as 81.65 (±7.72 BPM) and 81.5 (±8.1 BPM) as measured by the prototype and sphygmomanometer respectively. From the B&A plot of Figure 4.14, the bias between HR as measured by the two instruments is 0.2 BPM (95% CI = -0.3 to 0.6). On average therefore, the prototype measured 0.2 BPM higher than the sphygmomanometer. The systematic error is not significant as the line of equality is within the CI of the mean difference.

The upper and lower LoA are 2.2 BPM (95% CI = 1.3 to 3.0) and -1.9 BPM (95% CI = -2.7 to -1.0) respectively. This indicates that the results measured by the prototype may be 1.9 BPM below or 2.2 BPM above those measured by the sphygmomanometer. 95% of the differences between the measuring methods are within this range. From Equation (4.2), the LoA is found to be 4.1 BPM. The LoA does not exceed the priori criterion of 5 BPM. Therefore, the repeatability of the prototype in monitoring HR of patient B is acceptable. Hence the prototype is equivalent to the sphygmomanometer. Two data points have exceeded the LoA on the lower limit. This may be as a result of a possible error in the estimate due to sampling. From Equation (4.6), the percentage error is calculated to

be 5.03%. The HR differences are scattered around the bias, with some form of a straight-line pattern (variability).

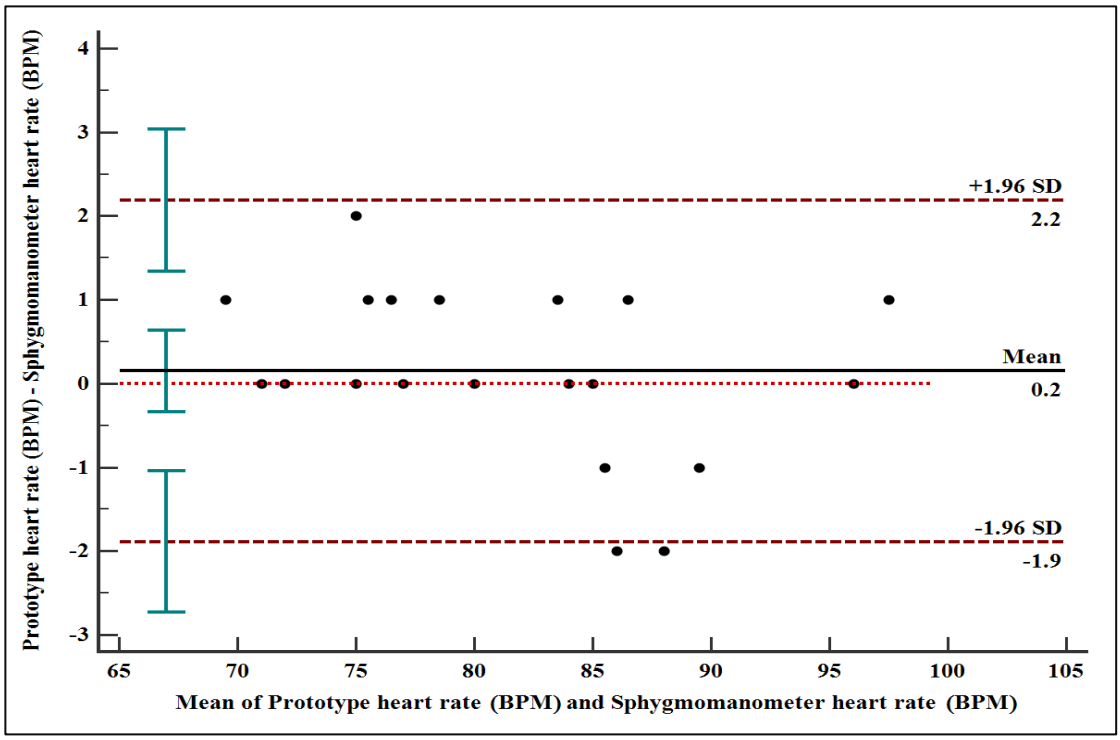

Figure 4.14: Bland-Altman HR Plot of Patient B in BPM

Figure 4.15 represents the same data as Figure 4.14, plotted as percentage of the differences. The bias is 0.2%, with varying variability across all measurements made. The agreement limits are from -2.2% to 2.7%. Most of the measurements are within the LoA thus the patient's HR is considered to be within a safe range.

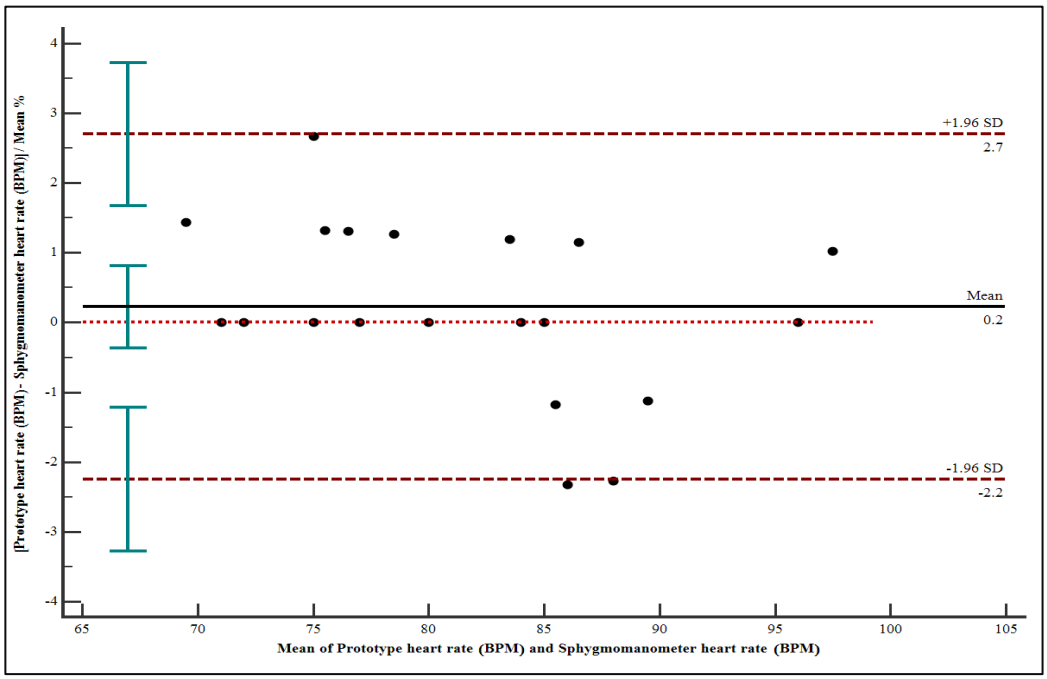

Figure 4.15: Bland-Altman HR Plot of Patient B as a Percentage

Figure 4.16 shows sphygmomanometer versus prototype readings for patient B monitored for 20 minutes. All the readings were in normal condition range (60 to 100 BPM) throughout the testing, indicating that the HR of B was healthy. The fluctuated points along the graph are due to a combination of factors similar to those of patient A.

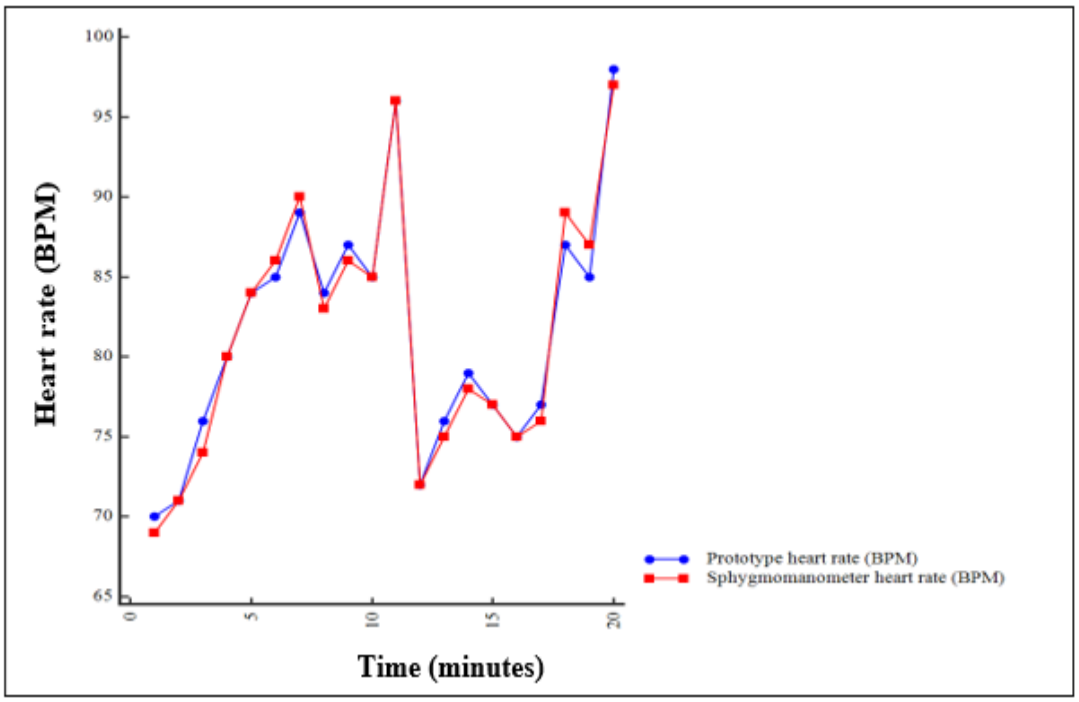

Figure 4.16: Heart Rate Profile for Patient B Monitored for 20 Minutes

4.2.5 BT Analysis for Patient C

The BT of patient C as monitored for 20 minutes by the two measuring instruments is detailed in Table 4.5.

Table 4.5: Body Temperature Data of Patient C as Monitored by the Two Measurement Methods

Time (minutes)	Prototype temperature (◦C)	Thermometer temperature (℃)
1.	37.26	37.24
2.	37.22	37.23
3.	37.22	37.22
4.	37.25	37.24
5.	37.25	37.23
6.	37.23	37.23
7.	37.25	37.25
8.	37.27	37.26
9.	37.26	37.25
10.	37.27	37.26
11.	37.29	37.29
12.	37.29	37.30
13.	37.30	37.30
14.	37.30	37.32
15.	37.31	37.32
16.	37.33	37.31
17.	37.34	37.34
18.	37.36	37.36
19.	37.37	37.36
20.	37.37	37.39

The prototype and thermometer temperature readings are related by Equation (4.9) and shown in Figure 4.17.

$$y = 0.904x + 3.589 \quad \text{..... 4.9}$$

The corresponding correlation coefficient (r) is 0.97. The gradient of Equation (4.9) is 0.904. This informs that there is a strong positive correlation between prototype and thermometer temperature readings. The constant 3.589 has units in °C and defines the core internal temperature at which the BT of patient C must be maintained for him to remain alive.

Significance level is, P < 0.001. The CoD (r^2) is 0.95 indicating that 95% of the BT measurements of patient C fall within the regression line. This gives a better goodness of

fit for the readings made by the two instruments. This in turn implies that subsequent readings have a 95% likelihood of following a similar trend.

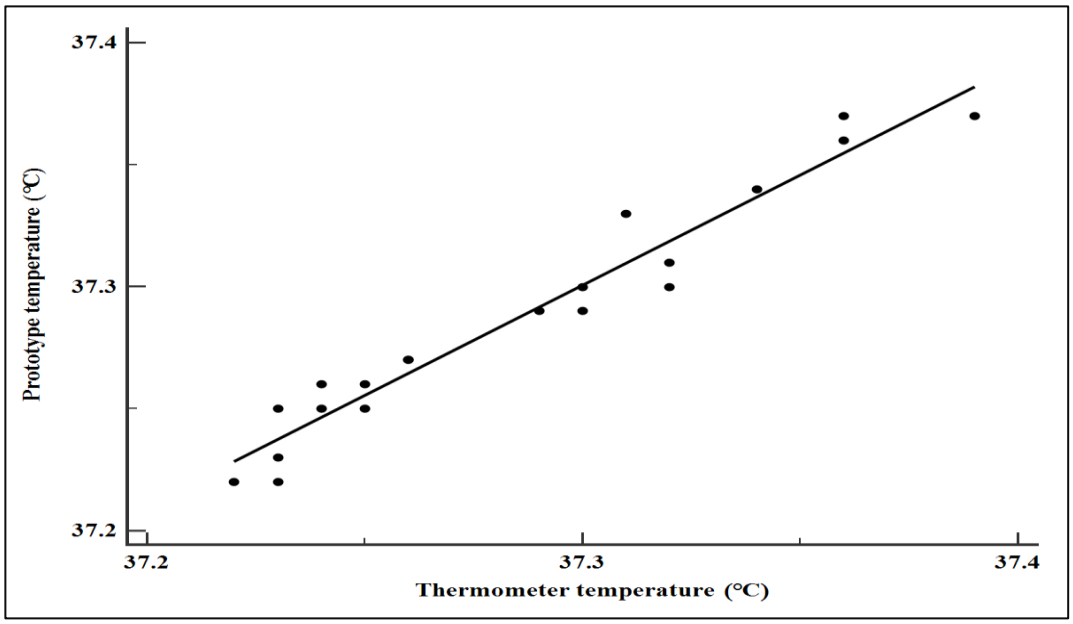

Figure 4.17: Scatter Plot of BT Monitoring for Patient C with Regression Line Indicated

The mean (±SD) BT of patient C is 37.29 (±0.05°C) for both measuring instruments as calculated from the data of Table 4.5. The B&A plot of the BT of patient C is shown in Figure 4.18. It is noted that the bias between the two methods is 0.002 °C (95% CI = -0.0036 to 0.0076). Therefore, on average the prototype measured 0.002 °C more than the thermometer. It is also noted that the systematic error (bias) is insignificant since the line of equality is within the CI of the mean difference.

0.025 °C (95% CI = 0.02 to 0.04) and -0.021 °C (95% CI = -0.031 to -0.012) are the upper and lower LoA respectively. This indicates that the results measured by the prototype may be 0.021°C below or 0.025°C above those measured by the thermometer. 95% of the differences between the methods are within this range. From Equation (4.3), the LoA is found to be 0.046°C. The LoA does not exceed the priori criterion of 0.2°C. Therefore, the repeatability of the prototype in monitoring BT of patient C is acceptable. Hence, the

prototype can substitute the thermometer in monitoring human BT. From Equation (4.4), the percentage error is 0.12%. The temperature differences are scattered around the bias, with some form of a straight-line pattern (variability). This is validated by the presence of the percentage error.

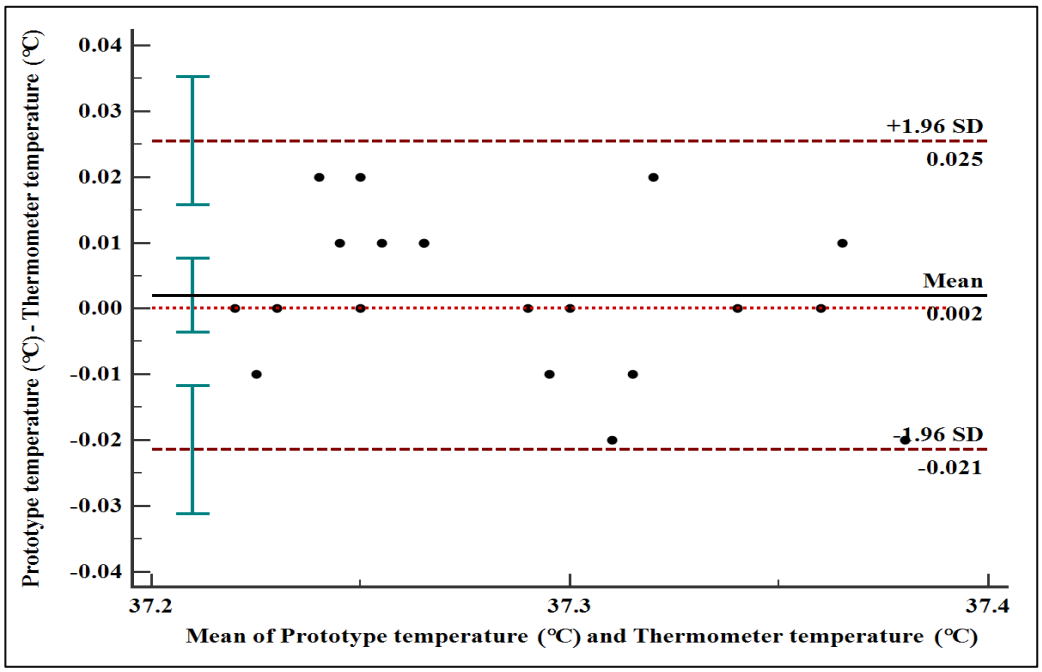

Figure 4.18: Bland-Altman BT Plot of Patient C in °C

Figure 4.19 represents the B&A percentage plot of the data in Table 4.5. The bias is 0.01% with varying variability across all the measurements. The agreement limits are from -0.06% to 0.07%.

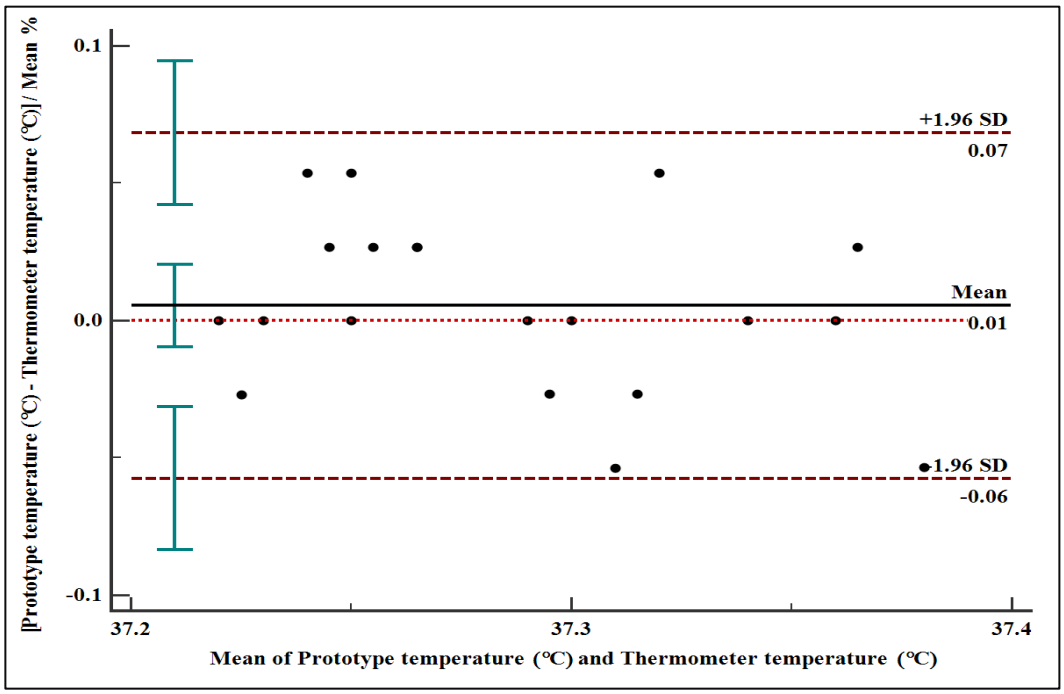

Figure 4.19: Bland-Altman BT Plot of Patient C as a Percentage

Figure 4.20 gives thermometer versus prototype temperature readings for patient C for a timeframe of 20 minutes. The BT of patient C was of normal status (36.5°C to 37.2°C) throughout the testing period. The fluctuated points along the graph are due to a combination of factors similar to those of patient A.

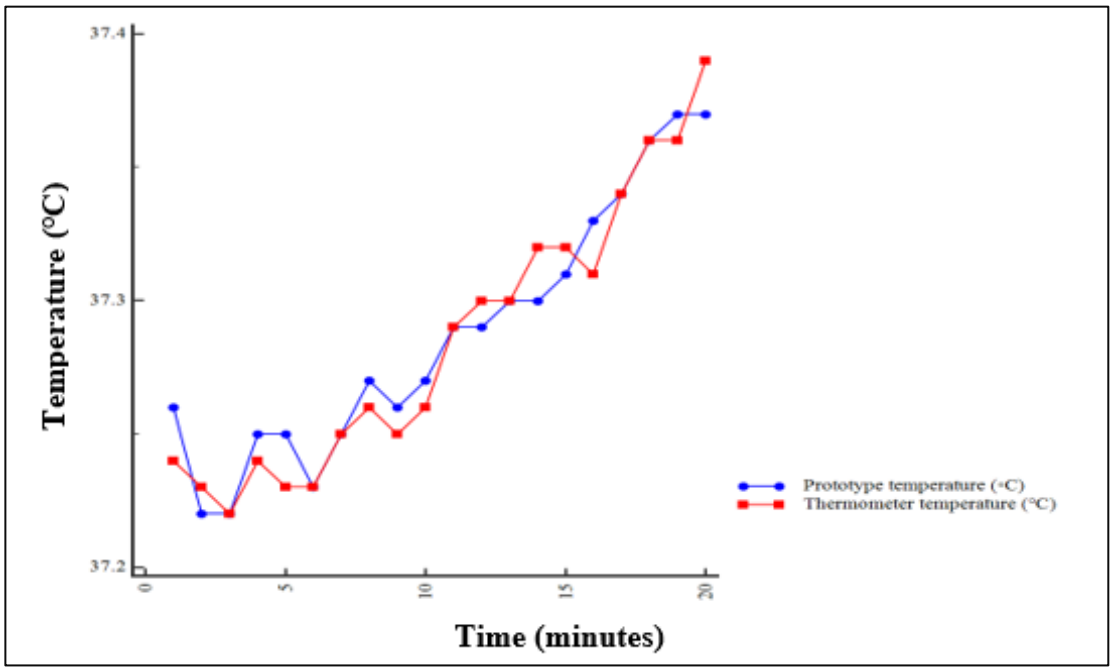

Figure 4.20: Temperature Profile for Patient C Monitored for 20 Minutes

4.2.6 HR Analysis for Patient C

Table 4.6 details the HR of patient C as recorded for 20 minutes with the two measuring instruments.

Table 4.6: Heart Rate Data of Patient C as Monitored by the Two Measurement Methods

Time (minutes)	Prototype heart rate (BPM)	Sphygmomanometer heart rate (BPM)
1.	72	70
2.	85	84
3.	64	65
4.	64	65
5.	64	65
6.	65	65
7.	76	74
8.	84	84
9.	62	62
10.	75	76
11.	73	72
12.	64	64
13.	77	76
14.	79	80
15.	76	76
16.	86	86
17.	87	86
18.	81	82
19.	84	84
20.	90	89

A scatter plot of the data in Table 4.6 shows that there exists a linear positive relation between the two instruments in monitoring the HR of patient C. This is shown in Figure 4.21 and is given by a correlation coefficient (r) of 0.99. The prototype and sphygmomanometer HR measurements are related by the straight line Equation (4.10).

$$y = 1.025x - 1.691 \quad \text{..... 4.10}$$

The correlation coefficient (r) is 0.99 and the gradient of Equation (4.10) is 1.025. This implies that there is a strong positive correlation between prototype and sphygmomanometer readings. The constant -1.691 has units in BPM and represents some specific HR at which the heart of patient C must beat for him to be alive.

Significance level is, P < 0.001. The COD (r^2) is 0.99 indicating that 99% of HR readings for patient C fall within the regression line. This gives a better goodness of fit for the readings made by the two instruments. This in turn implies that subsequent measurements have a 99% likelihood of following this trend thus providing a good measure of the accuracy of the prototype in monitoring HR.

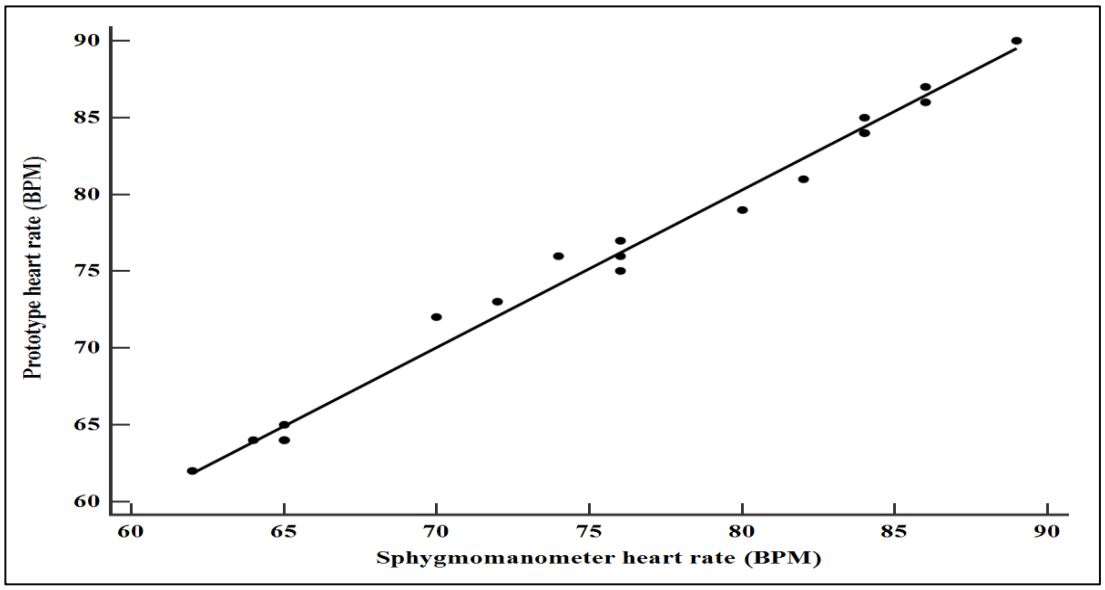

Figure 4.21: Scatter Plot of HR Monitoring for Patient C with Regression Line Indicated

The mean (±SD) HR of patient C was calculated to be 75.4 (±9.1 BPM) and 75.25 (±8.8 BPM) for the prototype and thermometer respectively. This is deduced from the data in Table 4.6. The B&A plot is shown in Figure 4.22. It is noted that the bias between the HR of C as measured by the prototype and the sphygmomanometer is 0.2 BPM (95% CI = -0.3 to 0.6). Hence, on average the prototype measured 0.2 BPM higher than the sphygmomanometer. This systematic error (bias) is not significant as the line of equality is within the CI of the mean difference.

2.1 BPM (95% CI = 1.3 to 2.9) and -1.8 BPM (95% CI = -2.6 to -0.1) are the upper and lower LoA respectively. This indicates that the results measured by the prototype may be

1.8 BPM below or 2.1 BPM above those measured by the sphygmomanometer. 95% of the differences between the measuring instruments are within this range. Using Equation (4.3), the LoA is calculated as 3.9 BPM. The LoA does not exceed the priori criterion of 5 BPM. Therefore, the repeatability of the prototype in monitoring HR of patient C is acceptable. The prototype is therefore a better replacement of the sphygmomanometer. Applying Equation (4.6), the percentage error is calculated to be 5.18%. The HR differences are scattered around the bias, with some form of a straight-line pattern (variability). This is validated by the presence of the percentage error.

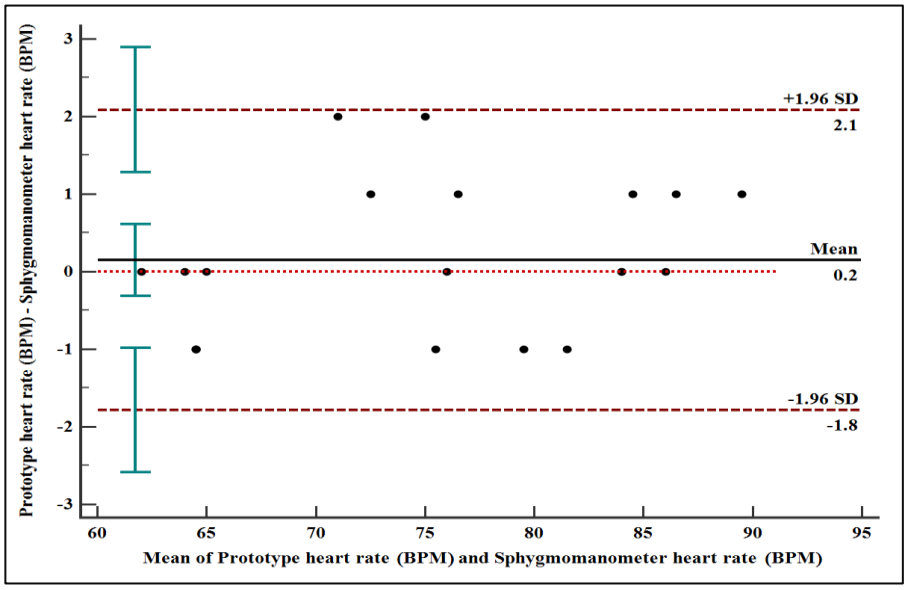

Figure 4.22: Bland-Altman HR Plot of Patient C in BPM

Figure 4.23 represents the B&A percentage plot of the data of Table 4.6. The bias is 0.2%, with varying variability across all the measurements. The agreement limits are from -2.5% to 2.8%.

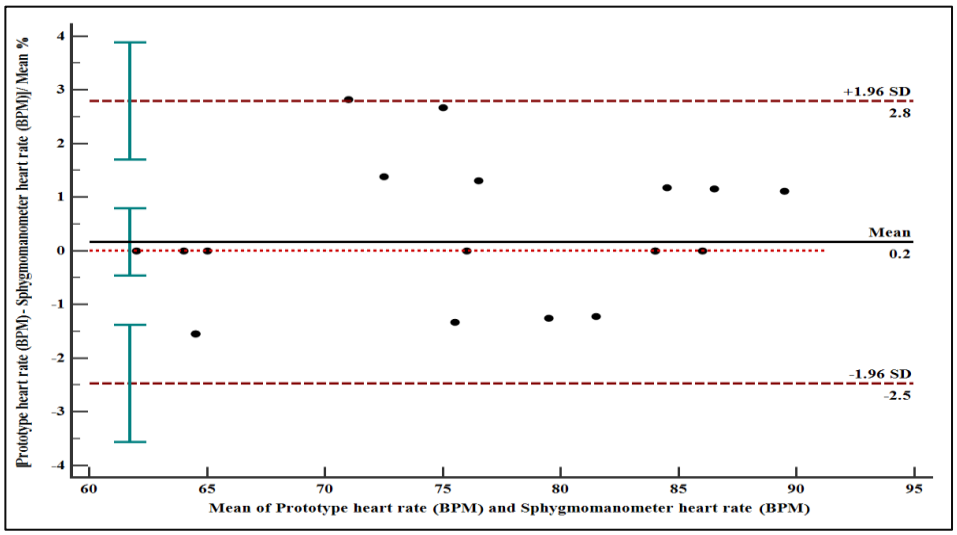

Figure 4.23: Bland-Altman HR Plot of Patient C as a Percentage

A plot of the HR of patient C as recorded by the prototype and the sphygmomanometer over a period of 20 minutes is shown in Figure 4.24. It is observed that patient C had his heart pulsating normally (60 to 100 BPM) throughout the testing time. The fluctuated points along the graph are due to a combination of factors similar to those of patient A.

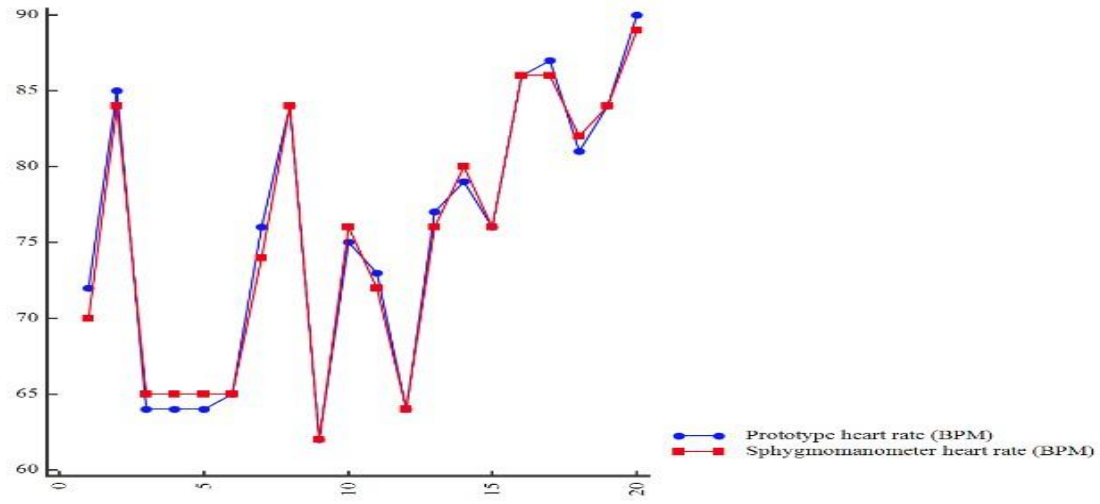

Figure 4.24: Heart Rate Profile For Patient C Monitored for 20 Minutes

4.2.7 BT analysis for patient D

Table 4.7 shows the variation of BT of patient D for 20 minutes as captured by the two monitoring instruments.

Table 4.7: Body Temperature Data of Patient D as Monitored by the Two Instruments

Time (minutes)	Prototype temperature (◦C)	Thermometer temperature (℃)
1.	36.57	36.60
2.	36.62	36.61
3.	36.62	36.61
4.	36.61	36.61
5.	36.63	36.64
6.	36.63	36.64
7.	36.66	36.67
8.	36.64	36.65
9.	36.66	36.66
10.	36.69	36.70
11.	36.69	36.69
12.	36.72	36.72
13.	36.73	36.72
14.	36.77	36.75
15.	36.76	36.76
16.	36.79	36.78
17.	36.79	36.81
18.	36.81	36.81
19.	36.80	36.81
20.	36.82	36.83

A scatter plot of the data of Table 4.7 results into a linear positive relation between the readings of the two methods of measuring the BT of patient D as depicted by Figure 4.25. Analysis of the data results in a correlation coefficient (r) of 0.99 and Equation (4.11).

$$y = 1.007x - 0.266 \quad \text{..... 4.11}$$

The gradient of Equation (4.11) is 1.007 implying that there is a strong positive correlation between prototype readings and thermometer readings. The constant -0.266 has units in

°C and represents the core internal temperature at which the body of patient D must be maintained for her to remain alive.

Significance level is, P < 0.001. The CoD (r^2) is 0.98 indicating that 98% of the BT readings of patient D fall within the regression line. This is interpreted to mean that there is a better goodness of fit for the measurements made by the two instruments. This in turn implies that subsequent measurements have a 98% likelihood of following the same trend. This gives a good measure of the accuracy of the prototype system in monitoring BT.

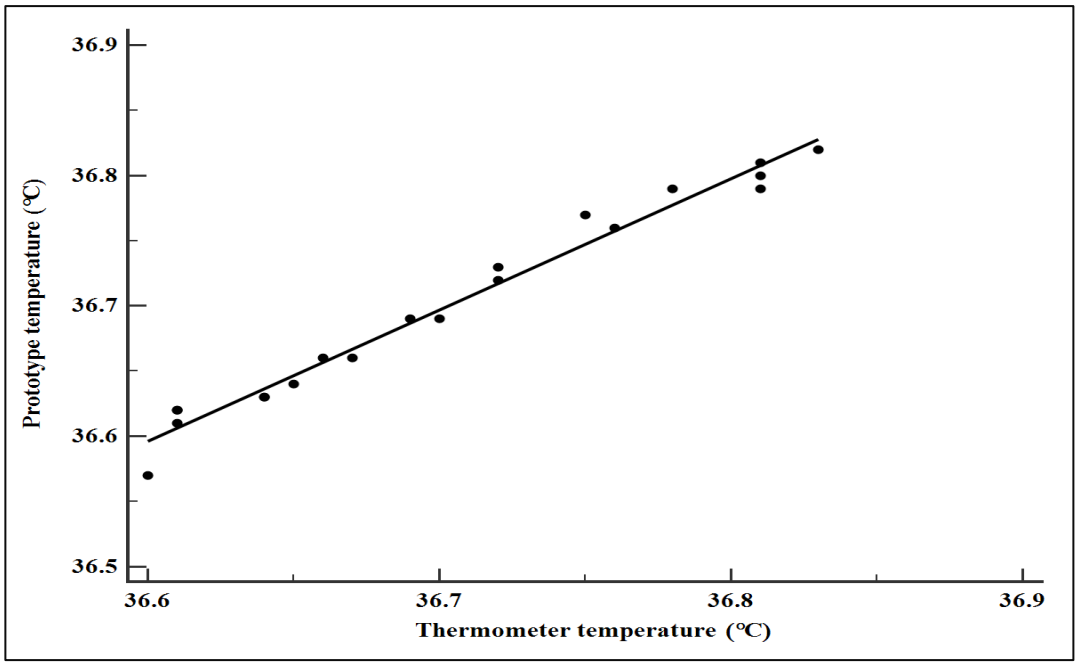

Figure 4.25: Scatter Plot of BT Monitoring for Patient D with Regression Line Indicated

With reference to Table 4.7, the mean (±SD) BT of patient D was determined to be 36.7 (±0.08°C) as measured by the prototype and thermometer instruments. The B&A plot is shown in Figure 4.26. The bias between the two methods is -0.003°C (95% CI = -0.008 to 0.002). On average the prototype measured 0.003°C lower than the thermometer. Systematic error (bias) is not significant, because the line of equality is within the CI of the mean difference.

0.020°C (95% CI = 0.010 to 0.030) and -0.026°C (95% CI = -0.036 to -0.016) are the upper and lower LoA respectively. This entails that the readings of the prototype may be 0.026°C below or 0.02°C above those measured by the thermometer. 95% of the differences between the two methods are within this range. Using Equation (4.3), the LoA is found to be 0.05°C. The LoA does not exceed the clinically acceptable precision of 0.2°C. Therefore, the repeatability of the prototype in monitoring BT is acceptable. The prototype may thus replace the thermometer in monitoring BT.

A single outlier present can be attributed to a possible error in the estimate due to sampling. From Equation (4.4), the percentage error is 0.13%. The temperature differences are scattered about the bias, in the form of a straight-line (variability). This is validated by the presence of the 0.13% error.

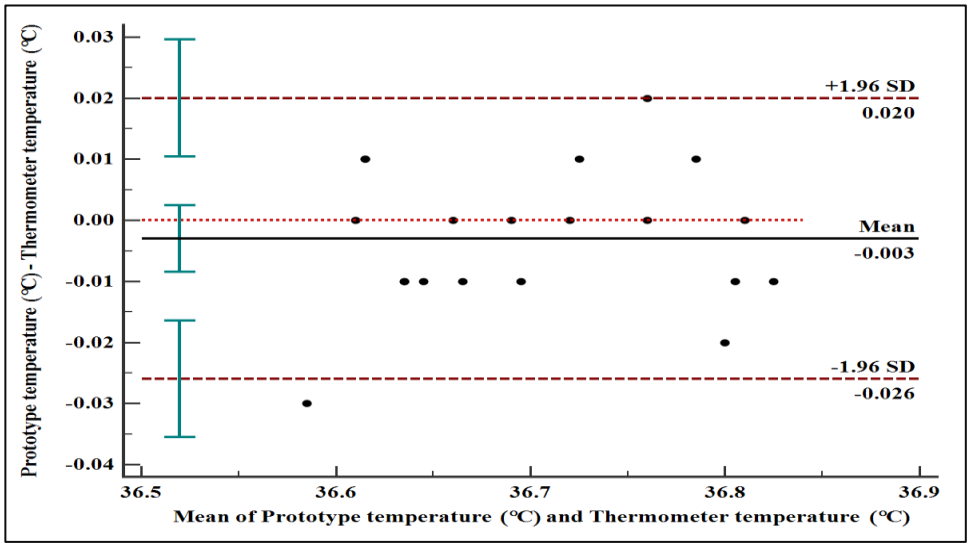

Figure 4.26: Bland-Altman BT Plot of Patient D in °C

Figure 4.27 shows the B&A percentage plot for the data of Table 4.7. The bias is -0.01%, with varying variability across all the measurements. The agreement limits are from -0.07% to 0.05%.

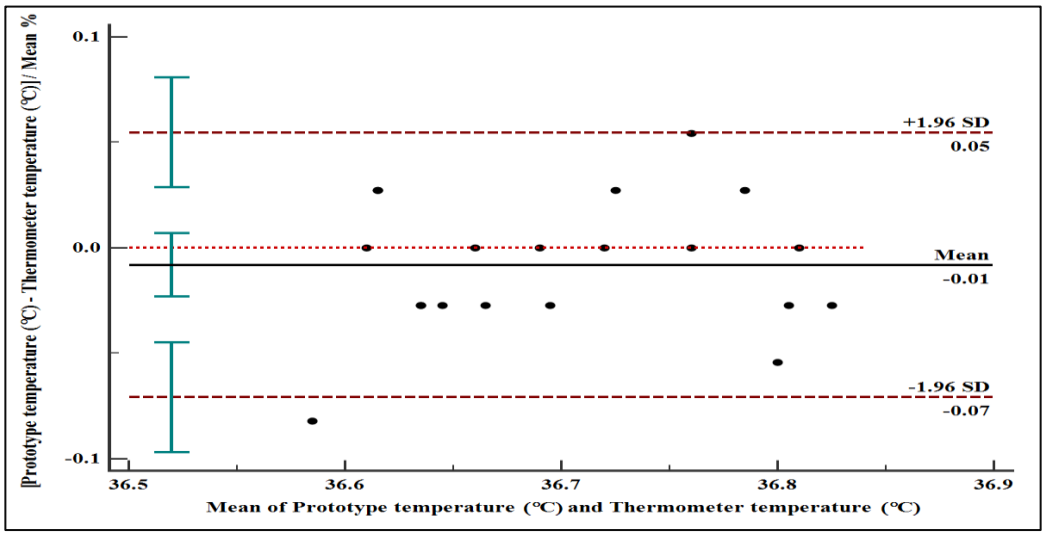

Figure 4.27: Bland-Altman BT Plot of Patient D as a Percentage

Figure 4.28 represents thermometer versus prototype BT readings for patient D as recorded for a period of 20 minutes of the experiment being carried out. The readings indicate that the BT of patient D was normal (36.5°C to 37.2°C) throughout the test period. The fluctuated points along the graph are due to a combination of factors similar to those of patient A.

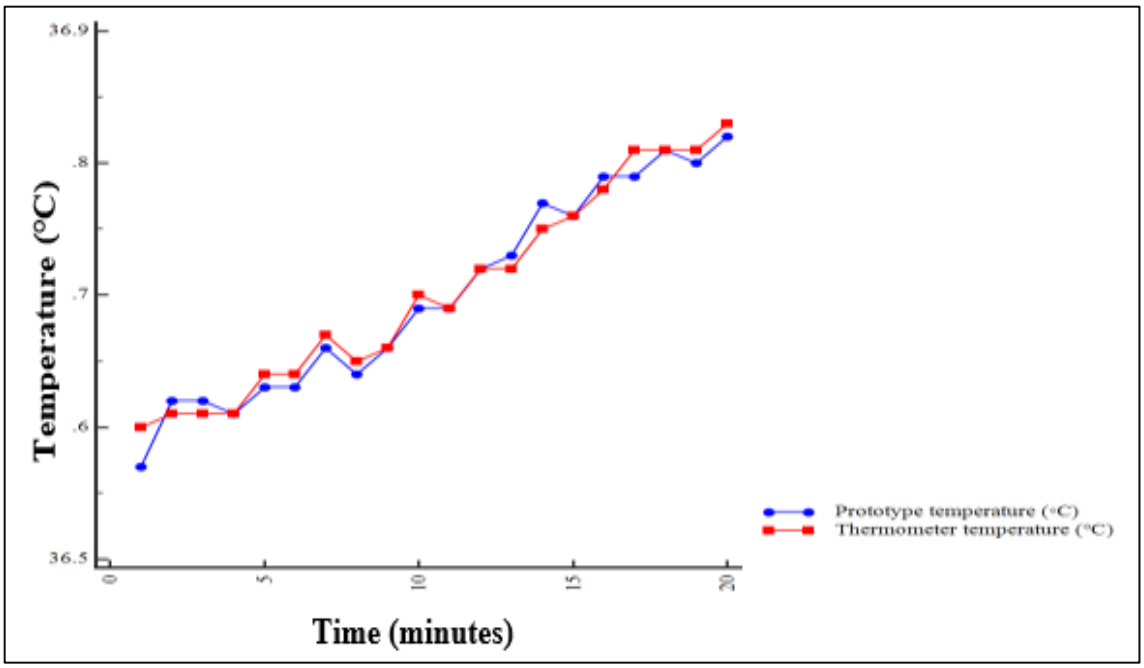

Figure 4.28: Temperature Profile for Patient D monitored for 20 Minutes

4.2.8 HR Analysis for Patient D

Table 4.8 details the variation of HR of patient D as captured for 20 minutes with the two measuring instruments.

Table 4.8: Heart Rate Data of Patient D as Monitored by the Two Instruments

Time (minutes)	Prototype heart rate (BPM)	Sphygmomanometer heart rate (BPM)
1.	75	74
2.	74	74
3.	67	68
4.	65	65
5.	67	68
6.	64	63
7.	66	68
8.	60	61
9.	89	90
10.	74	74
11.	63	63
12.	61	61
13.	69	70
14.	61	71
15.	80	82
16.	81	82
17.	85	84
18.	78	78
19.	76	76
20.	62	62

A scatter plot of the data of Table 4.8 is shown in Figure 4.29. Analysis of the data gives a correlation coefficient (r) of 0.96 and the straight line Equation (4.12).

$$y = 0.993x - 0.362 \quad \text{..... 4.12}$$

The gradient of Equation (4.12) is 0.993. This reveals that there is a strong positive correlation between readings made by the prototype against those of the sphygmomanometer. The -0.362 BPM constant defines some specific HR at which the heart of patient D must pulsate for her to be alive.

Significance level is, P < 0.001. The CoD (r^2) is 0.93 indicating that 93% of HR readings of patient D fall within the regression line. This gives a better goodness of fit for the readings made with the two instruments. Subsequent measurements therefore have a 93%

likelihood of following the same trend. This gives a good measure of the accuracy of the prototype system in monitoring HR.

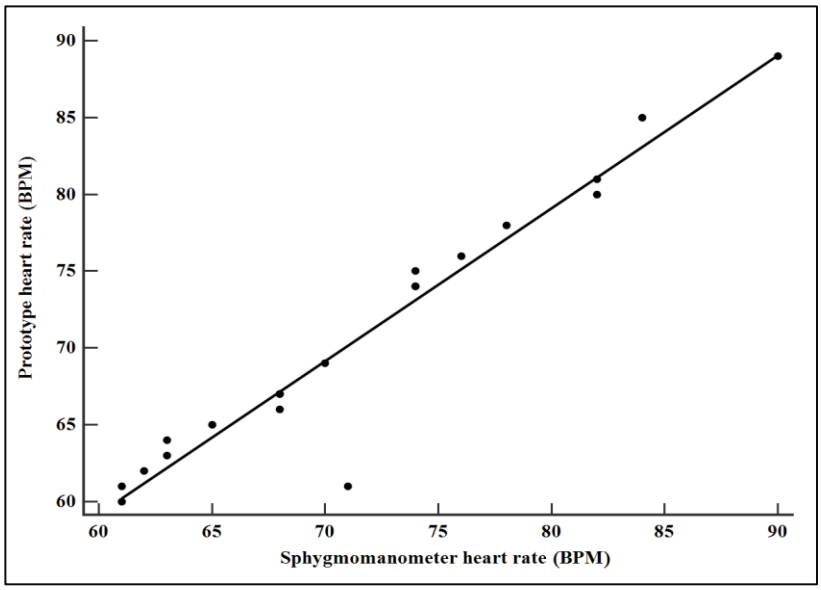

Figure 4.29: Scatter Plot of HR Monitoring for Patient D with Regression Line Indicated

As per Table 4.8, the mean (±SD) HR of patient D was found to be 70.85 (±8.6 BPM) and 71.7 (±8.4 BPM) as measured by the prototype and sphygmomanometer respectively. The B&A plot is shown in Figure 4.30. It is noted that the bias between HR as measured by the prototype and the sphygmomanometer instruments is -0.9 BPM (95% CI = -1.9 to 0.2). On average therefore, the prototype measured 0.9 BPM lesser than the sphygmomanometer. The systematic error is somewhat significant as the line of equality is almost approaching the 95% CI of the mean.

3.7 BPM (95% CI = 1.8 to 5.6) and -5.4 BPM (95% CI = -7.3 to 3.5) are the upper and lower LoA respectively. This indicates that the results measured by the prototype may be 5.4 BPM below or 3.7 BPM above those measured by the sphygmomanometer. 95% of the differences between the measuring methods are within this range. From Equation (4.3), the LoA is calculated to be 9.1 BPM. The LoA is so wide and greatly exceeds the

clinically acceptable precision of 5 BPM by 4.1 BPM. Therefore, the repeatability of the prototype in monitoring the HR of patient D is unacceptable. Inherent error in the measurement must have been prevalent. Applying Equation (4.6), the percentage error is calculated as 12.69%. The HR differences are scattered around the bias, in the form of a straight-line pattern (variability). This is validated by the presence of the percentage error.

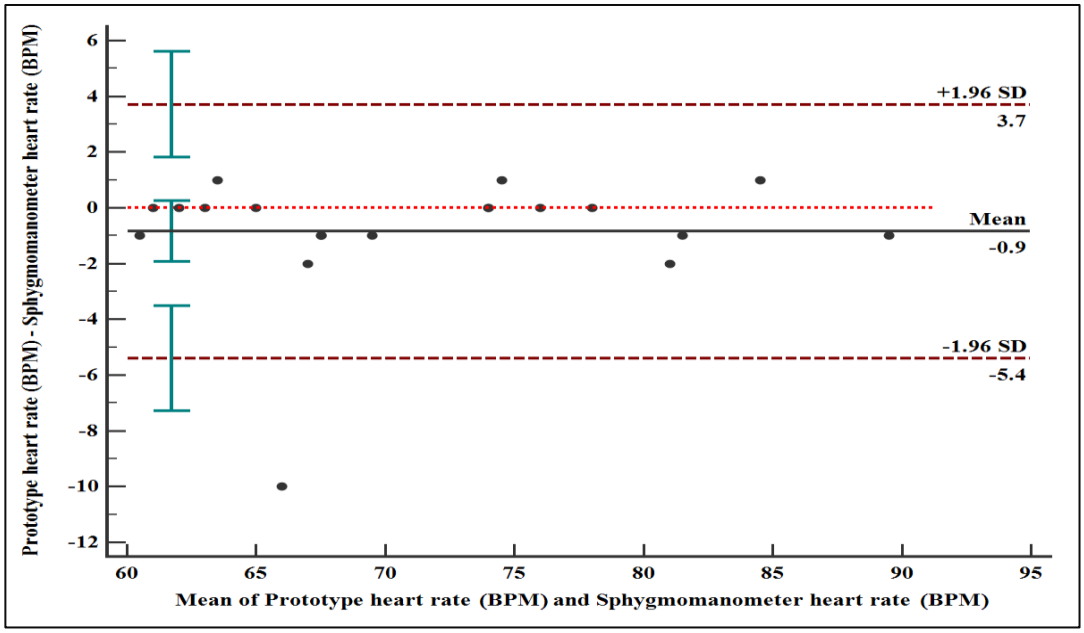

Figure 4.30: Bland-Altman HR Plot of Patient D in BPM

Figure 4.31 gives details of the B&A percentage plot of the data of Table 4.8. The bias or the mean difference is -1.2%, with varying variability across all the readings. The agreement limits are from -8.1% to 5.6%.

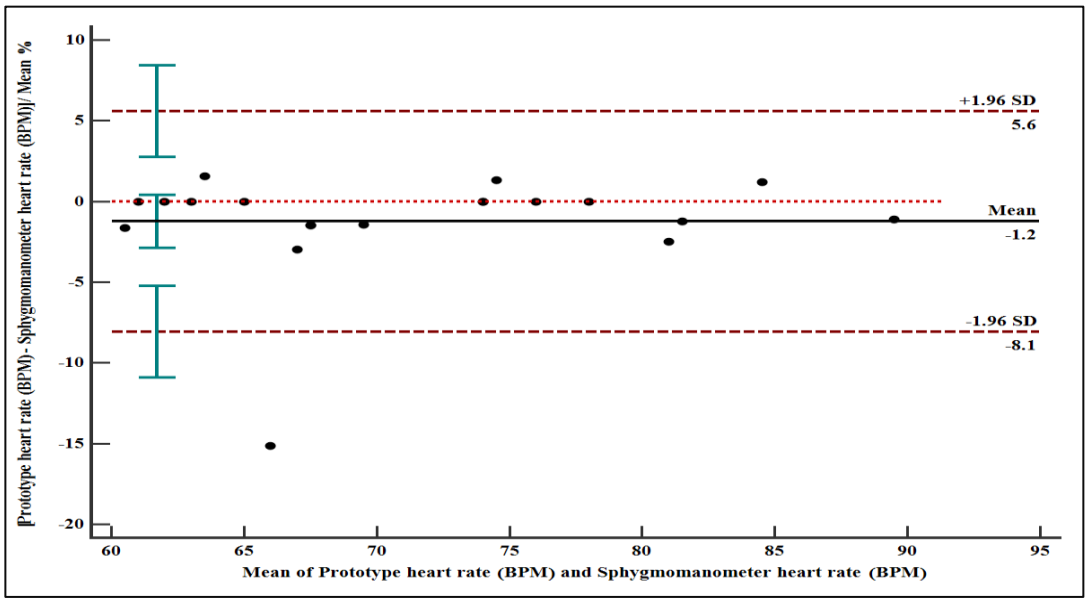

Figure 4.31: Bland-Altman HR Plot of Patient D as a Percentage

Figure 4.32 shows sphygmomanometer against prototype readings as monitored for a period of 20 minutes. It connotes that HR of patient D was pulsating normally during the time of the experiment. The fluctuated points along the graph are due to a combination of factors similar to those of patient A.

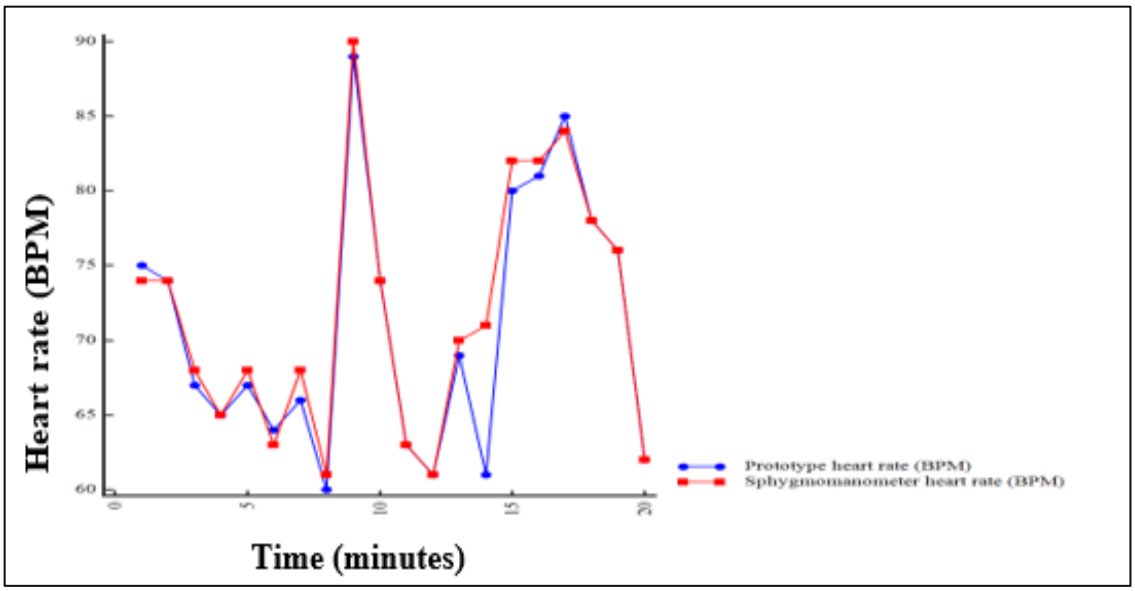

Figure 4.32: Heart Rate Profile for Patient D Monitored for 20 Minutes

CHAPTER FIVE

CONCLUSION AND RECOMMENDATION

5.1 Conclusion

From the findings of the study, it can be concluded that: There is a high positive correlation between the prototype and the established electronic clinical thermometer in monitoring the BT of patients as shown in Equation (4.2), Equation (4.7), Equation (4.9) and Equation (4.11). Secondly, there is a high positive correlation between the prototype and the standard electronic sphygmomanometer in monitoring the HR of patients as shown in Equation (4.5), Equation (4.8), Equation (4.10) and Equation (4.12). Also, the systematic error or bias is negligibly small/tiny for all the four BT and HR patients under consideration. This is in relation to the ±0.5°C and ±5 BPM clinical conditions determined a priori. This indicates that the prototype measurements are accurate in relation to the true values as read by the standard methods. In addition, there are clinically narrow limits of agreement in the four cases considered hence rendering the three methods essentially equivalent and in agreement. Lastly, there is no increase in variability of the differences as the magnitude of the measurements increased. This is observed from the Bland-Altman percentage plots where the data points are distributed in a similar manner as those of the unit plots.

In summary, the measurements by the prototype in remote monitoring of BT and HR are in agreement with those of the established clinical thermometer and sphygmomanometer methods. Hence, the prototype is equivalent to the two instruments and can therefore replace them or any other system used for the remote monitoring of BT and HR of patients respectively.

5.2 Recommendations and Future Work

Further studies may be carried out to modify and improve upon the prototype model by interfacing it with additional biosensors so as to enable it non-invasively monitor more

physiological parameters, especially those that still require direct contact between the patient and the medical practioner such as blood pressure, blood glucose level, blood oxygen level, respiration rate, level of intravenous fluid usage and many more. This is of extreme necessity due to the onset of the novel COVID-19 virus and other opportunistic diseases. In addition, more patients from across the world may be included in the study. The increase in the sample size may lead into more precise results. This is so because random errors are not so problematic, especially in studies with large samples.

Lastly, consideration may be made to integrate artificial intelligence (AI) into RPM. The incorporation of AI algorithms will augment the potential of RPM by analyzing vast amounts of patient data to detect trends, anomalies and potential issues.

REFERENCES

Adams M.J., Briscoe B.J. and Johnson S.A. (2007). Friction and lubrication of human skin. Tribology Letters. **26**(3): 239-253.

Aruna S., Godfrey S. and Sasikumar S. (2016). Patient Health Monitoring System (PHMS) using Internet of Things (IoT) Devices. International Journal of Computer Science and Engineering Technology, **7**(3): 68-73.

Avram R., Tison G.H., Aschbacher K., Kuhar P., Vittinghoff E., Butzner M., Runge R., Wu N., Pletcher M.J., Marcus G.M. and Olgin J. (2019). Real-world heart rate norms in the Health eHeart study.NPJ Digital Medicine. **2**(58):1-10.

Balli S., Shumway K. R. and Sharan S. (2023). Physiology, Fever. In: StatPearls. StatPearls Publishing. https://www.ncbi.nlm.nih.gov/books/NBK562334/. Accessed January 25, 2024.

Bhattacharya J., Kanjilal P. and Muralidhar V. (2001). Analysis and characterization of photo-plethysmographic signal. IEEE Transactions on Biomedical Engineering, **48**(1): 5-11.

Billman E. (2011). Heart rate variability - A historical perspective. Frontiers in Physiology, **86**(2): 1-13.

Bronzino J.D. and Diakides N.A. (2013). Medical infrared imaging. CRC Press, USA.

Buttà C., Tuttolomondo A., Di Raimondo D., Milio G., Miceli S., Attanzio T. and Pinto A. (2013). The supraventricular tachycardias: Proposal of a diagnostic algorithm for the narrow complex tachycardias. Journal of Cardiology, **61**(4): 247–255.

Charkoudian N. (2003). Skin blood flow in adult human thermoregulation: how it works, when it does not, and why. Mayo Clinic Proceedings. **78**(5): 603-612.

Chen H., Chen A. and Chen C. (2020). Investigation of the Impact of Infrared Sensors on Core Body Temperature Monitoring by Comparing Measurement Sites. Sensors. **20**(10): 2885.

Dereniak E.L. and Boreman G.D. (1996). Infrared Detectors and Systems. John Wiley & Sons Inc.,New York.

Diakides M., Bronzino J.D. and Peterson D.R. (2013). Medical Infrared Imaging: Principles and Practices. CRC Press, Boca Raton, Florida. P.p 19-1-19-32.

Dobesch A. and Poliak J. (2013). IR Thermometer with Automatic Emissivity Correction. Radioengineering, **22**(4): 1301-1306.

Egejuru E. (2008). Microcontroller Based Heart Rate Monitor and Arrhythmia Detector. MSc. Thesis. University of Illinois - Urbana Champaign, USA.

Ellebrecht D.B., Gola D. and Kaschwich M. (2022). Evaluation of a Wearable in-Ear Sensor for Temperature and Heart Rate Monitoring: A Pilot Study. Journal of Medical Systems. **46**(91):1-10.

Gao G. Q. (2003). Computerized Detection and Classification of Five Cardiac Conditions. Ms. C. Thesis. Auckland University of Technology, Auckland, New Zealand.

Geneva I., Cuzzo B., Fazili T. and Javaid W. (2019). Normal Body Temperature: A Systematic Review. Open Forum Infectious Diseases. **6**(4): 1-7.

Giavarina D. (2015). Understanding Bland Altman Analysis. Biochemia Medica. **25**(2): 141-151.

Gratt B.M. (2013). Medical Infrared Imaging: Infrared imaging applied to dentistry. CRC Press, Boca Raton, USA, 20-1 - 20-9.

Gupta H.S., Sharma A. and Sogani D. (2009). Wireless Heartbeat Monitor. National Conference on Recent Developments in Computing and its Applications (NCRDCA). Proceedings of a conference, August 12-13, New Delhi, Delhi, India. P.p 366 - 370.

Guyton A.C. and Hall J.E. (2011). Guyton and Hall textbook of medical physiology. Saunders Elsevier, Philadelphia.

Hanneman K. S. (2008). Design, Analysis and Interpretation of Method-Comparison Studies. AACN Advanced Critical Care. **19**(2): 223-234.

Janke D., Kagelmann N., Storm C., Maggioni M.A., Kienast C., Gunga H.C. and Opatz O. (2021). Measuring Core Body Temperature Using a Non-invasive, Disposable Double-Sensor During Targeted Temperature Management in Post-cardiac Arrest Patients. Frontiers in Medicine. **8** (666908):1-9.

Jayasree K. V., Shaija J. P., Nampoori N. P. V., Girijavallabhan P. C. and Radhakrishnan P. (2007). A Simple and Novel Integrated Opto-electronic System for Blood Volume Pulse Sensing and Heart Rate Monitoring. International Journal of Optomechatronics, **1**(4): 392-403.

Jin G., Zhang X., Fan W., Liu Y. and He P. (2015). Design of Non-Contact Infra-Red Thermometer Based on the Sensor of MLX90614. The Open Automation and Control Systems Journal. **7**(1): 8-20.

Jones B.F. (1998). A reappraisal of the use of infrared thermal image analysis in medicine. IEEE Transactions on Medical Imaging. **17**(6): 1019-1027.

Kansara P., Dhar R., Shah R., Mehta D. and Raut P. (2021). Heart Rate Measurement. Journal of Physics: Conference series. **1831**(1): 1-11.

Karaduman I. (2014). Global challenges for the world. OBRONNOŚĆ. Zeszyty Naukowe, **2**(10): 45 - 58.

Kellogg D.L. Jr. (2006). In vivo mechanisms of cutaneous vasodilation and vasoconstriction in humans during thermoregulatory challenges. Journal of Applied Physiology. **100**(5): 1709-1718.

Koehler M.J., Vogel T., Elsner P., Konig K., Buckle R. and Kaatz M. (2010). In vivo measurement of the human epidermal thickness in different localizations by multiphoton laser tomography. Skin Research and Technology. **16**(3): 259-264.

Lasanen R. (2015). Infrared thermography in the evaluation of skin temperature: Applications in musculoskeletal conditions. Ph.D. Thesis. University of Eastern Finland, Kuopio, Finland.

Meola C. (2012). Infrared Thermography Recent Advances and Future Trends. Bentham Science Publishers, Oak Park III.

Modest M.F. (2003). Radiative Heat Transfer. Academic Press, Boston.

Moorthy C.G. and Sankar G.U. (2019). Planck's Constant and Equation for Magnetic Field Waves. Natural and Engineering Sciences. **4**(2): 107-113.

Moraes J., Rocha M., Vasconcelos G., Vasconcelos Filho J., de Albuquerque V. and Alexandria A. (2018). Advances in Photoplethysmography Signal Analysis for Biomedical Applications, Sensors, **18**(6): 1894

Musellim B., Borekci S., Uzan G., Ali Sak Z. H., Ozdemir S. K., Altinisik G., Altunbey S. A., Sen N., Kilinc O., Yorgancioglu A. and Duration for Patient Examination Working Group of Turkish Thoracic Society. (2017). What should be the appropriate minimal duration for patient examination and evaluation in pulmonary outpatient clinics, Annals of thoracic medicine, **12**(3): 177–182.

Ng D.K., Chan C.H., Lee R.S. and Leung L.C. (2005). Non-contact infrared thermometry temperature measurement for screening fever in children. Annals of Tropical Paediatrics. **25**(4): 267–275.

Ng D. K., Chan C., Chan E.Y., Kwok K., Chow P., Lau W.F. and Ho J.C. (2005). A brief report on the normal range of forehead temperature as determined by noncontact, handheld, infrared thermometer. American Journal of Infection Control. **33**(4): 227–229.

Oleg P., Valentyna V. and Pavel V. (2021). Health Care as a Global Problem of Humanity and its Relationship with other Global Problems. Humanities Studies: Collection of Scientific Papers. **7**(84): 39-47.

Parsons K. (2014). Human Thermal Environments, CRC Press, Boca Raton, Florida.

Pennes H.H. (1998). Analysis of tissue and arterial blood temperatures in the resting human forearm. Journal of Applied Physiology. **85**(1): 5-34.

Perpetuini D., Filippini C., Cardone D. and Merla A. (2021). An Overview of Thermal Infrared Imaging Based Screenings during Pandemic Emergencies. International Journal of Environmental Research and Public Health. **18**(6):3286.

Peter L., Vorek I., Massot B., Bryjova I. and Urbanczyk T. (2016). Determination of Blood Vessels Expandability; Multichannel Photoplethysmography. IFAC-PapersOnLine, **49**(25): 284–288.

Ring E.F. and Ammer K. (2012). Infrared thermal imaging in medicine. Physiological Measurement. **33**(3): 33-46.

Sammito S. and Böckelmann I. (2016). Factors influencing heart rate variability. International Cardiovascular Forum Journal. **6**(10): 18-22.

Silver F.H., Freeman J.W. and DeVore D. (2001). Viscoelastic properties of human skin and processed dermis. Skin Reseach and Technology. **7**(1): 18-23.

Sudhindra F., Annarao S. J., Vani R. M. and Hunagund P. V. (2016). Development of Real Time Human Body Temperature (Hypothermia & Hyperthermia) Monitoring & Alert System with The Global System for Mobile Communications (GSM) & Global Positioning System (GPS). International Journal of Innovative Research in Science, Engineering and Technology, **5**(6): 9355-9362.

Sudianto A., Jamaludin Z., Rahman A.A.A., Novianto S. and Muharrom F. (2020). Smart Temperature Measurement System for Milling Process Application Based on MLX90614 Infrared Thermometer Sensor with Arduino. Journal of Advanced Research in Applied Mechanics. **72**(1): 10-24.

Sullivan G. and Edmondson C. (2008). Heat and temperature. Continuing Education in Anaesthesia Critical Care & Pain. **8**(3): 104-107.

Sun Y. and Thakor N. (2016). Photoplethysmography Revisited: From Contact to Noncontact, From Point to Imaging. IEEE Transactions on Biomedical Engineering. **63**(3): 463-477.

Sviridova N. and Sakai K. (2015). Human photoplethysmogram: new insight into chaotic characteristics, Chaos, Solitons and Fractals. **77**(1): 53-63.

Tiwari R., Kumar R., Malik S., Raj T. and Kumar P. (2021). Analysis of Heart Rate Variability and Implication of Different Factors on Heart Rate Variability. Current Cardiology Reviews. **17**(5): 1-10.

Wahyuningtya T. D., Astuti D. S., Rahmawati T. and Soetjiatie L. (2023). Design and analysis of non-contact temperature monitoring system for temperature measurement in the Tympanic membrane. In: The 11th International Conference on Theoretical and Applied Physics: The Spirit of Research and Collaboration

Facing the CO-19 Pandemic. Conference Proceedings. 27–28 October 2021. Surabaya, Indonesia.

Valentini M. and Parati G. (2009). Variables Influencing Heart Rate. Progress in cardiovascular diseases, **52**(1): 1-9.

Warwick R. and Wiliams P.L. (1973). Gray's anatomy. Longman, London.

Yaffe D. B. (2020). “Thermometer Guns on Coronavirus Front Lines are Notoriously not Accurate”. The New York Times. https://www.nytimes.com/2020/02/14/business/coronavirus-temperature-sensor-guns.html . Accessed June 6, 2023.

Youssef A. A. A., Wouters F., Vranken J., de Korte-de Boer D., Smit-Fun V., Duflot P., Beaupain M-H., Vandervoort P., Luca S., Aerts J. M. and Vanrumste B. (2020). Vital Signs Prediction and Early Warning Score Calculation Based on Continuous Monitoring of Hospitalised Patients Using Wearable Technology, Sensors, **20**(22): 6593.

Zaki R. (2017). Validation of Instrument Measuring Continuous Variable in Medicine. Advances in Statistical Methodologies and Their Application to Real Problems. P.p. 217-237.

APPENDICES

Appendix I: General Structure of a Bland-Altman Plot

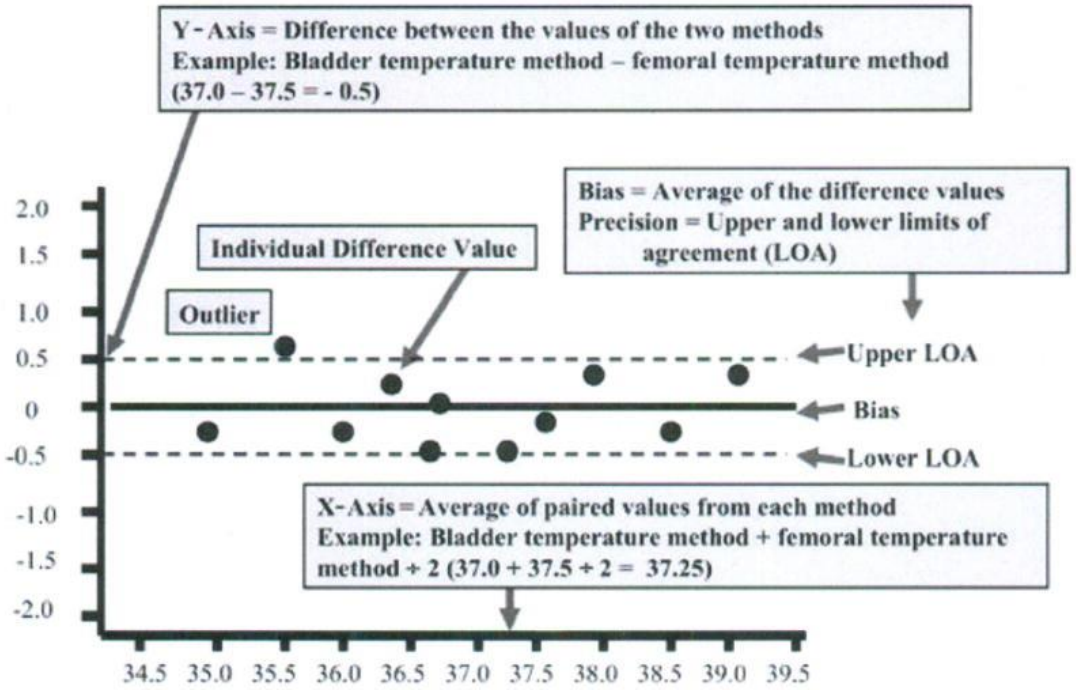

Figure A_1: Structure of a Bland-Altman plot with explanation of elements, using a comparison of temperatures (°C) obtained with two temperature methods (bladder; femoral). (Hanneman., 2008)

Appendix II: Definitions of Terms Used in a Method-Comparison Study

Term	Definition
Bias	The mean (overall) difference in values obtained with two different methods of measurement
Confidence Limit	Range within which 95% of the differences from the bias are expected to be
Limits of Agreement	Confidence limits for the bias. Upper limit of agreement (Upper LoA in Figure A_1) is computed as bias + 1.96SD, where SD is that of the bias. The lower limit of agreement (Lower LoA in Figure A_1) is computed as bias − 1.96SD. Upper LoA − lower LoA = confidence limit
Percentage Error	Proportion between the magnitude of measurement and the error in measurement
Precision	The degree to which the same method produces the same results on repeated measurements (repeatability); the degree to which values cluster around the mean of the distribution of values (e.g., width of confidence interval)
Standard Deviation	A measure of variability of the individual differences

Appendix III: Bivariate Sample Mathematical Modelling Formulae Used with Bland-Altman Plot

I. Bias

The bias between two tests is measured by the mean of the differences given by:

$$\bar{d} = \frac{1}{n}\sum_{k=1}^{n} d_k$$

II. Limits of Agreement

Limits of agreement between two tests are defined by a 95% prediction interval of a particular value of the difference computed as:

$$\bar{d} \pm 1.96 S_d$$

Where: $S_d = \sqrt{\frac{1}{n-1}} \sum_{k=1}^{n} (d_k - \bar{d})^2$

- **Variances**

Variances for the bias and LoA for normally distributed differences is given by:

Bias: $\widehat{Var}(\bar{d}) = \frac{S_d^2}{n}$

LoA: $\widehat{Var}(\bar{d} \pm 1.96 S_d) = (\frac{1}{n} + \frac{1.96^2}{2(n-1)}) S_d^2$

- **Confidence Intervals**

CI's for the bias and LoA for normally distributed differences is given by:

95% CI's for the mean difference (the bias) is,

$$\bar{d} \pm t_{1-\propto/2,n-1} \sqrt{\widehat{Var}}(\bar{d})$$

95% CI's for the LoA are given by:

$$(\bar{d} - 1.96 S_d) - t_{1-\propto/2,n-1} \sqrt{\widehat{Var}}(\bar{d} \pm 1.96 S_d)$$

$$(\bar{d} + 1.96 S_d) + t_{1-\propto/2,n-1} \sqrt{\widehat{Var}}(\bar{d} \pm 1.96 S_d)$$

Appendix IV: Prototype Code

BT & HR Program

```
#include <TinyGPS.h>// gps library
#include <OneWire.h// ds1820 library
#include “U8glib.h”// lcd screen library
//gsm
String number1 = +254720777320”;
String number2 = “+254737060680”;
String sendMes = “ ”;
//Wifi
String sendValue = “>0, 0, 0, 0<”;
String ratesS = “0”;
String temperatureS = “0”;
String flatS = “0”;
String flonS = “0”;
Int counter = 0;
//gps
TinyGPS gps;
float flat, flon;
bool newData = false;
char temp_string [5];
char bpm_string [5];
U8GLIB_ST7920_128×64 u8g (42, 41, 40, U8G_PIN_NONE);
//heart rate
int pulsePin = 0; //analog pin A0
float rates;
float flat, flon;
volatile  int    BPM; // HR
volatile   int   Signal;
```

```
volatile int IBI = 600;
volatile boolean Pulse = false;
Volatile Boolean QS = false;
//temperature
OneWire ds (8) ; //pin 8
float temperature = 37;
#include <TinyGPS.h>// gps library
#include <OneWire.h// ds1820 library
#include “U8glib.h”// lcd screen library
//gsm
String number1 = +254720777320”;
String number2 = “+254737060680”;
String sendMes = “ ”;
//Wifi
String sendValue = “>0, 0, 0, 0<”;
String ratesS = “0”;
String temperatureS = “0”;
String flatS = “0”;
String flonS = “0”;
Int counter = 0;
//gps
TinyGPS gps;
float flat, flon;
bool newData = false;
char temp_string [5];
char bpm_string [5];
U8GLIB_ST7920_128×64 u8g (42, 41, 40, U8G_PIN_NONE);
//heart rate
int pulsePin = 0; //analog pin A0
float rates;
```

```
volatile  int    BPM; // HR
volatile   int   Signal;
volatile int IBI = 600;
volatile boolean Pulse = false;
Volatile Boolean QS = false;
//temperature
OneWire ds (8) ; //pin 8
float temperature = 37;
Void setup ( )  {
Serial.begin (115200) ; //computer screen
Serial1.begin (9600) ; //gsm
Serial2.begin (9600) ; //gps
Serial3.begin (9600) ; //wifi
Delay (1000) ;
InterruptSetup ( ) ;
u8g.setFont (u8g_font_8×13) ;
u8g.setColorIndex (1) ;
u8g.firstPage ( );
do       {
u8g.drawStr (1, 13, “patient Health”) ;
u8g.drawStr (1, 27,” Monitoring”) ;
} while (u8g.nextPage ( ) ) ;
delay(3000);
u8g.firstPage ( ) ;
do     {
    u8g.drawStr (1, 13, “                    “);
    u8g.drawStr (1, 27, “                    “);
   u8g.drawStr (1, 13, “Initializing….”);
} while ( u8g.nextPage ( )    ) ;
delay (1000) ;
```

```
u8g.firstPage ( );
do  {
   u8g.drawStr (1, 13, “                    ”);
   u8g.drawStr (1, 27, “                    “);
   u8g.drawStr (1, 13, “Getting Data….”);
}  while  (  u8g.nextPage  ( )  );
Delay (4000) ;
}
u8g firstPage ( ) ;
void loop ( ) {
temperature = takeTemperature ( ) ;
If    (QS - - true)    {
     Rates = BPM;//HR
     QS = false;
}
gpsread ( ) ;
ratesS – String (rates) ;
temperatureS – String (temperature) ;
flatS – String (flat, 6) ;
flonS – String (flon, 6) ;
sendMes – ratesS +  “  BPM  “  +  temperatureS  +  “  *C   “  +  flatS  +  “ , “  +  flonS;
if   ( (temperature < - 36) && (rates < - 60 ) ) {
draw (“bradycardia”,”hypothermia”) ;
   sendMes  + - “    bradycardia and hypothermia” ;
/*
Sendtext (number1, sendMes) :
Sendtext (number2, sendMes) ;
*/
Serial.println (sendMes) ;
```

```
}
else if  ( (temperature < - 36) && (rates < - 100 ) )  {
      draw ( “normal rate” , “hypothermia” ) ;
sendMes +- “  normal rate and hypothermia”;
/*
sendtext (number1,     sendMes);
sendtext (number2,     sendMes);
*/
Serial . printIn (sendMes);

}
else if  ( ( temperature < - 36) && (rates > 100) ) {
   draw ( “tachycardia”, “hypothermia” ) ;
sendMes + - “ tachycardia and hypothermia” ;
/*
sendtext (number1,     sendMes);
sendtext (number2,     sendMes);
*/
Serial . printIn (sendMes);
}
else if  ( ( temperature < - 37) && ( rates < - 60) ) {
     draw ( “bradycardia”, “normal temp” ) ;
     sendMes + - “       bradycardia and normal temp” ;
     /*
    sendtext (number1, sendMes) ;
    sendtext (number2, sendMes );
    */
     Serial . printIn (sendMes) ;
}
else if  ( ( temperature < - 37) && ( rates < - 100) ) {
```

```
      draw ( “normal rate”, “normal temp” ) ;
}
else if  ( ( temperature < - 37) && ( rates >  100) ) {
      draw ( “tachycardia”, “normal temp” ) ;
      sendMes + - “       tachycardia and normal temp” ;
sendtext (number1, sendMes) ;
sendtext (number2, sendMes );
*/
Serial . printIn (sendMes) ;
}
else if  ( ( temperature > 37) && ( rates < -  60) ) {
      draw ( “bradycardia”, “hyperthermia” ) ;
          sendMes + - “  bradycardia and hyperthermia” ;
/*
sendtext (number1, sendMes) ;
sendtext (number2, sendMes );
*/
Serial . printIn (sendMes) ;
}
else if  ( ( temperature > 37) && ( rates < -  100) ) {
    draw ( “normal rate”, “hyperthermia” ) ;
    sendMes + - “    normal rate and hyperthermia” ;
    /*
   sendtext (number1, sendMes) ;
   sendtext (number2, sendMes );
   */
   Serial . printIn (sendMes) ;
}
else if  ( ( temperature > 37) && ( rates >  100) ) {
   draw ( “tachycardia”, “hyperthermia” ) ;
```

```
      sendMes + - “    tachycardia and hyperthermia” ;
/*
      sendtext (number1, sendMes) ;
      sendtext (number2, sendMes );
*/
  Serial . printIn (sendMes) ;
}
SendValue – “ > “ + rates + “,” + temperatureS + “,” + flatS + “,” + flonS + “<”;
if (counter < -0 ){
  Serial3.print (sendValue);
  Serial.printIn (sendValue);
  counter-8;
  }
//delay (10000);
counter--;
}
float takeTemperature ( ) {
   byte i;
   byte present – 0;
   byte type_s;
   byte data [ 12 ];
   byte addr [ 8 ];
  float Celsius;
if ( !ds.search (addr) )  {
   //Serial.println (“No more addresses.”);
   //Serial.println ( );
   ds.reset_search ( );
   return;
}
if (OneWire::crc8 (addr, 7)    ! – addr [7])  {
```

```
   // Serial.println ("CRC is not valid!") ;
   return;
}
//   Serial.printIn ( );
ds.reset ( );
ds.select (addr) ;
ds.write (0×44,  1);                //start conversion, with parasite power on at the end
unsigned long int time1 – millis ( );
delay (1000);
//we might do a ds.depower ( ) here, but the reset will take care of it.
present – ds.reset ( );
ds.select (addr);
ds.write (0×BE);
 for  ( i – 0; I < 9; i++ )  {                // we need 9 bytes
   data[i] – ds.read ( );
}
int16_t raw – (data [1] << 8)  |  data [0];
if  (type_s)  {
   raw – raw << 3;  // 9 bit resolution default
   if  (data [7] - - 0×10)  {
         // "count remain" gives full 12 bit resolution
         raw – (raw & 0×FFF0) + 12 – data [6];
         }
} else {
   byte cfg – (data [4] & 0×60);
   // at lower res, the low bits are undefined, so let's zero them
   if  (cfg - - 0×00) raw – raw & ~7;  // 9 bit resolution, 93.75 ms
   else if  (cfg - - 0×20) raw – raw & ~3;  // 10 bit resolution, 187.5 ms
   else if  (cfg - - 0×40) raw – raw & ~1;  // 11 bit resolution, 375 ms
   //// default is 12 bit resolution, 750 ms conversion time
```

```
}
celsius – (float) raw / 16.0;
return Celsius;
}
void sendtext (String num, String mes)  {
  Serial1.printIn ( “AT” );
  delay (100);
  Serial1.printIn ( “AT+CMGF-1”);
  delay (200);
Serial1.printIn ( “AT+CMGs-\””);
Serial1.printIn (num);
Serial1.printIn (“\””);
delay (500);
Serial1.printIn (mea);
delay (500);
Serial1.printIn ( (char) 26);
void gpsread ( )  {
    newData – false;
    //ss.listen ( );
    for (unsigned long start – millis ( ); millis ( ) – start < 1000;)
   {
      while (Serial2.available ( ) )
         {
            char c – Serial2.read ( );
            if  (gps.encode (c) ) // Did a new valid sentence come in?
               newData – true;
           }
}
if   (newData)
{
```

```
        gps.f_get_position (&flat, & flon);
        flat _ _ TinyGPS: :GPS_INVALID_F_ANGLE  ?  flat 0.0 : flat – flat, 6;
        flon _ _ TinyGPS: :GPS_INVALID_F_ANGLE  ?  flon 0.0 : flon – flon, 6;
  }
}
void draw (char bpmdc [5], char tempdc [5] )  {
   u8g . firstPage ( ) ;
        do  {
           u8g.drawStr (1, 13, "                    ");
           u8g.drawStr (1, 27, "                    ");
            u8g.drawStr (1, 13, "        "BPM :");
         dtostrf (rates,  3,  0,  bpm_string);
         u8g.drawStr (53, 13, bpm_string);
         u8g.drawStr (1, 27,   "Temp. :");
         dtostrf (temperature,  3,  2,  temp_string);
         u8g.drawStr (53, 27,   temp_string );
         u8g.drawStr (100, 27,   "*C");
         u8g.drawStr (1, 60,   "                    ");
         u8g.drawStr (1, 60,   "tempdc);
         u8g.drawStr (1, 48,   "                    ");
         u8g.drawStr (1, 48,    bpmdc);
         }  while (u8g.nextPage ( ) );
```

Interrupt Program

```
         volatile int rate [10];
         volatile unsigned long sampleCounter – 0;
         volatile unsigned long lastBeatTime – 0;
         volatile int P – 512;
         volatile int T – 512;
         volatile int thresh – 512;
         volatile int amp – 100;
```

```
volatile boolean firstBeat – true;
volatile boolean secondBeat – false;
void interruptSetup ( )  {
  // Initializes Timer2 to throw an interrupt every 2Ms.
  TCCR2A – 0×02;          // DISABLE PWM ON DIGITAL PINS 3 AND 11, AND GO INTO CTC MODE
  TCCR2B – 0×06;          // DON'T FORCE COMPARE, 256 PRESCALER
  OCR2A - 0×7C;           // SET THE TOP OF THE COUNT TO 124 FOR 500Hz SAMPLE RATE
  TIMSK2 - 0×02;          // ENABLE INTERRUPT ON MATCH BETWEEN TIMER2 AND OCR2A
  sei ( );                // MAKE SURE GLOBAL INTERRUPTS ARE ENABLED
  }
// THIS IS THE TIMER 2 INTERRUPT SERVICE ROUTINE.
// Timer 2 makes sure that we take a reading every 2 milliseconds
  ISR (TIMER2_COMPA_vect)  {                    // triggered when Timer2 counts to 124
      cli ( );                                  // disable interrupts while we do this
  Signal – analogRead (pulsePin);               // read the Pulse Sensor
   SampleCounter + - 2;                         // keep track of the time in mS with this variable
  int   N – sampleCounter – lastBeatTime;       // monitor the time since the last beat to avoid noise
      // find the peak and the trough of the pulse wave
      if (Signal < thresh && N > (IBI / 5)  *  3)  {  // avoid dichrotic noise by waiting 3/5 of last IBI
        if   (Signal < T)  {                    // T is the trough
```

```
                    T – Signal;                         // keep track of lowest
point in pulse wave
        }
    }
        if  (Signal  >  thresh && Signal  >  P)  {     // thresh condition helps avoid noise
                P – Signal;                             // P is the peak
           }                                            // keep track of highest point in pulse
wave
        // NOW IT'S TIME TO LOOK FOR THE HEART BEAT
        // signal surges up in value every time there is a pulse
         if (N > 250)  {                                    // avoid high frequency noise
          if (   (Signal > thresh)  &&  (Pulse - - false)  &&  (N > (IBI / 5)  *3)   )   {
                Pulse – true;
                IBI – sampleCounter – lastBeatTime;         // measure time between
beats in Ms
                lastBeatTime – sampleCounter;               // keep track of time for next
pulse
                if   (secondBeat)   {                       // if this is the second beat, if
secondBeat - - TRUE
                secondBeat – false;                         // clear secondBeat flag
                for  (int I -0;  I  < - 9;  I ++)   {       // seed the running total to get
a realistic BPM at startup
                        rate [i] – IBI;
                        }
                }
                if  (firstBeat)   {                         // if it's the first time we
found a beat, if firstBeat - - TRUE
                        firstBeat – false;                  // clear secondBeat flag
                        for  (int  I – 0;  I  < - 9; i++)  {        // seed the running total to get
a realistic BPM at startup
```

```
                rate [i] – IBI;
            }
        }
        If (firstBeat)  {                   // if it's the first time we
found a beat, if firstBeat - - TRUE
        firstBeat – false;                  // clear firstBeat flag
        secondBeat – true;                  // set the second beat flag
        sei ( );                            // enable interrupts again
        return;                             // IBI value is unreliable so
discard it
    }
    // keep a running total of the last 10 IBI values
    word runningTotal – 0;                  // clear the runningTotal
variable
    for (int I – 0; I < - 8; i++)           // shift data in the rate array
      rate [i] – rate [i + 1];              // and drop the oldest
IBI value
            runningTotal +- rate [i]        // add up the 9 oldest IBI
values
            }
            rate [9] – IBI;                 // add the latest IBI to the rate
        array
            runningTotal +- rate [9];       // add the latest IBI to
        runningTotal
            runningTotal /- 10;             //average the last 10 IBI
        values
            BPM – 60000 / runningTotal;     // how many beats can fit into
        a minute? That's BPM!
            QS – true;                      // set Quantified Self flag
            // QS FLAG IS NOT CLEARED INSIDE THIS ISR
```

```
                }
            }
            if (Signal < thresh && Pulse - - true)   {
                Pulse – false;                          // rest the Pulse flag so we
can do it again
                amp – P – T;                            // get amplitude of the pulse
wave
                thresh – amp / 2 +T;                    // set thresh AT 50% of the
amplitude
                P – thresh;                             // reset these for next time
                 T – thresh;
            }
            if (N > 2500)   {                           // if 2.5 seconds go by
without a beat
            thresh – 512;                               // set thresh default
            P – 512;                                    // set P default
            T – 512;                                    // set T default
            lastBeatTime – sampleCounter;               // bring the lastBeatTime up
to date
            firstBeat – true;                           // set these to avoid noise
            secondBeat – false;                         // when we get the heartbeat
back
          sei ( );                                      // enable interrupts when
you're done!
            } // end isr
```

Appendix V: Picture of Prototype Setup with Results Displayed on the LCD